Gradient-based optimization of permanent-magnet assemblies for any objective

Andrea Roberto Insinga⬤* and Rasmus Bjørk⬤

Department of Energy Conversion and Storage, Technical University of Denmark - DTU, Anker Engelunds Vej 1, Kgs. Lyngby DK-2800, Denmark

We introduce a semianalytical optimization method that can be applied to find the optimal magnetization for any permanent-magnet system regarding the desired field or objective. Our approach is based on the Landau-Lifshitz equation, which is normally employed to simulate micromagnetic systems. Instead, we recognize that the same mathematical formalism is also applicable to the optimization of macroscopic magnetic assemblies. This point of view has the advantage of being easy to intuitively visualize and thus is also easy to implement. Our approach can also be seen as a special case of the adjoint method, which is a gradient-based constrained optimization method. However, most studies applying the adjoint method to magnet design adopt the point of topology optimization, where the magnetic permeability tensor field depends on the design variables, making the problem highly nonlinear. Instead, we restrict to the less general problem of optimizing the direction of the magnetization in any point of a given design region. Our strategy leads to a more robust and computationally efficient algorithm since the underlying problem is intrinsically simpler. Additionally, since the integration of the underlying magnetostatic equations is performed numerically, the method is still very flexible and versatile. Previously, an equivalent method has been considered only for solving the magnetic inverse problem. In the present work, we fully demonstrate its effectiveness by presenting several prototypical optimization problems and we discuss the strengths and limitations of the approach in relation to the existing optimization methods.

I. INTRODUCTION

Permanent magnets are used in a number of applications, both in scientific and technological areas. Among these, some of the most significant are [1] electric motors, electric generators, accelerator magnets, nuclear magnetic resonance (NMR) devices, magnetic resonance imaging (MRI) scanners, and magnets for other biomedical purposes [2]. In all the applications it is critical to optimize the magnetic system so that it will generate a magnetic field that will result in the best performance for the considered application.

An aspect to consider is how the design optimization problem is formulated. A problem can be thought of being composed of two sides: the optimization objective and the optimization variables. The objective is generally expressed in terms of the magnetic field over a given field region. The difficulty of the problem depends on how the objective depends on the field, linear dependence being the simplest case.

A similar reasoning applies to the dependence of the magnetic field on the optimization variables. Let us consider topology optimization, one of the most widely

employed optimization approaches [3–6]. Here, the optimization variables determine the arrangement of materials in the design area. This is achieved by making the permeability tensor $\underline{\underline{\mu}}$ in any point **x** be dependent on the values of the design variable fields. This optimization approach is very versatile: it can be applied with any class of optimization objective, and also in the presence of nonlinear constitutive **B-H** relations [7]. However, the optimization problem considered by topology optimization approaches is intrinsically difficult to solve, because of the highly nonlinear dependence of the field with respect to $\underline{\underline{\mu}}(\mathbf{x})$.

Besides the optimization problem, the other aspect to consider is the mathematical technique used to perform the optimization. One way to classify the methods is based on whether or not they use the gradient for smoothly evolving the variables towards the optimal configuration. Gradient-free approaches, being purely numerical, are generally not very computationally efficient and it can be prohibitive to apply them to three-dimensional magnet design problems.

Gradient-based methods are a family of optimization approaches that use the analytical expression of the derivative of the optimization objective to construct a more efficient and robust optimization scheme. However, calculating the derivative of the objective with respect to the design variables may, in general, prove to be a challenging

---

*aroin@dtu.dk

task. The adjoint method addresses this issue by considering the dual of the original problem. The idea can be thought of as an application of the method of Lagrange multipliers, where the governing equation of the system, i.e., the state equation, is interpreted as a constraint. Thus, instead of calculating the derivative explicitly, it is obtained as the solution of the dual of the original problem. For example, for the case of magnetostatics in the absence of free currents, the state equation is Poisson's equation applied to the magnetic scalar potential. Since this problem is self-adjoint, the adjoint method assumes a particularly simple form.

This approach has been successfully applied to the optimization of permanent-magnet systems, such as in the works of Suess and co-workers [8–10], or by Lee and co-workers [11,12], or others [13]. In these studies, the derivative of the optimization objective with respect to the magnetic field is calculated analytically. The derivative of the field with respect to the design variables is then obtained by solving a partial differential equation that is formally equivalent to the state equation. In several studies based on this method, the considered problem is that of topology optimization, meaning that the value of the design variables at a point determines whether the point is occupied by a given material or not, e.g., 1 for magnet and 0 for air [8,10]. The same idea can be applied to the optimization of multimaterial designs, including iron, magnets, coils, and air [11], or also permanent magnets magnetized in different directions, i.e., segmented permanent-magnet assemblies [4].

The method discussed in the present paper belongs to this family of gradient-based optimization schemes. However, instead of optimizing the topology, we focus on the problem of optimizing the direction of the magnetization vector $\mathbf{M}(\mathbf{x})$ in any point $\mathbf{x}$ of the region occupied by permanent-magnet material. In other words, the magnetization field itself is chosen as a design variable. The same choice of design variable is adopted in Ref. [9] for solving the magnetic inverse problem, i.e., finding the magnetization that would generate a certain prescribed field in a given region. In the present work, we apply the same idea to any kind of design-optimization objective.

By assuming this perspective, the resulting optimization scheme becomes much more transparent and easy to understand. In fact, in this work we introduce an intuitive physical interpretation of the gradient terms involved in the optimization procedure. For example, the gradient of the optimization objective with respect to the unknown magnetization, i.e., the design variable, is analogous to the concept of effective field in the context of micromagnetics.

We consider the permeability tensor $\underline{\underline{\mu}}$ to be known, and we assume the constitutive **B-H** relation to be linear at any point. With these assumptions, we take advantage of the linearity of the field with respect to the design variable. This property, together with analytical calculation of the gradient of the objective with respect to the field, makes the underlying optimization problem much easier to solve than the topology optimization problems mentioned above.

We also assume that the norm of the magnetization vector is known, since this is determined by the choice of permanent-magnet material. This is a suitable approach for optimization permanent-magnet assemblies, where typically the grade of the permanent magnets are known from the application, and the optimal magnetization direction is to be determined. After this has been determined, the magnet assembly can then be segmented into individual pieces. Rather than imposing the normalization condition as a constraint, we incorporate it directly into the gradient-descent scheme, which thus becomes analogous to the Landau-Lifshitz equation, the governing equation of micromagnetic systems. Thanks to this parallelism between magnet design and micromagnetics, and to the fact that we assume a restricted problem for which the permeability tensor is known, the implementation of the optimization procedure is greatly simplified.

The approach described below can also be thought of as an extension to nonlinear objectives of the "virtual magnet" framework discussed in Refs. [14] and [15]. In the present study, we consider the case of continuous magnetization distributions that vary smoothly in space, as well as segmented systems composed by a finite number of uniformly magnetized parts. We provide a significant number of relevant examples from different applications. The results demonstrate the efficacy and wide applicability of this optimization framework to any kind of magnet design problems.

A. Notation

In this work we will denote vectors with bold font, as in $\mathbf{v}$. Space-dependent vector fields will be indicated with their input arguments between round brackets, as in $\mathbf{H}(\mathbf{x})$, where $\mathbf{x}$ shall denote a generic point of space. Rank-2 tensors will be denoted by double underlining, as in $\underline{\underline{\mu}}$. The input argument of tensor fields will also be denoted between round brackets, as in $\underline{\underline{\mu}}(\mathbf{x})$.

We will consider scalar nonlinear functionals denoted with calligraphic font, as in $\mathcal{S}$. The input argument of these functionals will be a vector field, such as $\mathbf{H}(\mathbf{x})$. The input argument of a functional will be indicated between square brackets, as in $\mathcal{S}[\mathbf{H}]$.

We will use the first-order derivative of a functional $\mathcal{S}$ with respect to its argument. Since the input argument of $\mathcal{S}$ is a function (specifically a vector field), the most rigorous notation is that used for functional derivatives. However, for simplicity in this work we will simply use the same notation commonly used for the ordinary gradient of multivariate functions, i.e., $\nabla_{\mathbf{H}}\mathcal{S}$. If the gradient is evaluated at the starting point $\mathbf{K}$, we will use $(\nabla_{\mathbf{H}}\mathcal{S})_{\mathbf{K}}$ to indicate this.

Finally, we consider operators having vector fields both as input and output argument. Nonlinear operators will be denoted with bold font and with their input argument between square brackets, as in $\mathbf{Q}[\mathbf{M}]$. Instead, linear operators will simply be denoted as the rank-2 tensors, as in $\underline{\underline{N}}$. The input argument of such operators will simply be juxtaposed on its right side. For example, if the operator $\underline{\underline{N}}$ is applied to the vector field $\mathbf{M}(\mathbf{x})$, we will use $\underline{\underline{N}}\,\mathbf{M}$ to indicate this.

B. Governing equations

In this work we consider magnetostatic systems [16], which are governed by Ampere's law,

$$\nabla \times \mathbf{H} = \mathbf{J} \tag{1}$$

and Gauss' law for magnetism

$$\nabla \cdot \mathbf{B} = 0, \tag{2}$$

where $\mathbf{H}$, $\mathbf{B}$, and $\mathbf{J}$ denote the magnetic field, magnetic flux density, and electric current density, respectively. The fields $\mathbf{B}$ and $\mathbf{H}$ are related to the magnetization $\mathbf{M}$ by the following equation:

$$\mathbf{B} = \mu_0(\mathbf{H} + \mathbf{M}), \tag{3}$$

where μ_0 is the magnetic permeability of vacuum. The constitutive relation between $\mathbf{B}$ and $\mathbf{H}$ is assumed to be linear, as expressed by

$$\mathbf{B} = \underline{\underline{\mu}}\mathbf{H}, \tag{4}$$

where $\underline{\underline{\mu}}$ is the permeability tensor. The linearity assumption is justified in a wide variety of relevant situations. An extensive discussion of the validity of this assumption is given in Sec. IV-A of Ref. [15].

II. CONTINUOUS MAGNETIZATION CASE

A. Optimization objective and effective field

We consider a problem where permanent magnets are placed in a region R_m, and have to generate a field in a region denoted by R_g. This latter region is typically an air gap. The two regions are assumed to be nonoverlapping. The optimization objective is to maximize or minimize a nonlinear functional $\mathcal{S}$, which depends on the magnetic field over R_g, which is denoted by $\mathbf{H}$. The magnetization field, $\mathbf{M}$, over R_m is the design-optimization variable of our problem, i.e., determining the optimal magnetization direction within the permanent magnets. Because of this, in the region R_m we are assuming $\mu = \mu_0$. In all the other regions, we assume the constitutive relation expressed by Eq. (4), where the permeability tensor is possibly space

dependent, i.e., $\underline{\underline{\mu}} = \underline{\underline{\mu}}(\mathbf{x})$, but it is assumed to be known, i.e., not an optimization variable. We also assume that the current density is zero everywhere $\mathbf{J} = \mathbf{0}$.

With these assumptions, the field $\mathbf{H}$ depends linearly on the magnetization field over R_m:

$$\mathbf{H} = \underline{\underline{N}}\mathbf{M}, \tag{5}$$

where the linear operator $\underline{\underline{N}}$ corresponds to applying the demagnetization tensor. In explicit notation this means

$$\mathbf{H}(\mathbf{x}) = \int_{R_m} dV' \, \underline{\underline{N}}(\mathbf{x}, \mathbf{x}') \, \mathbf{M}(\mathbf{x}'). \tag{6}$$

Here, the demagnetization tensor is defined in a slightly unconventional way, in the sense that it takes into account the magnetic reaction of all the regions of the geometry outside R_m, where the constitutive relation is $\mathbf{B} = \underline{\underline{\mu}}\mathbf{H}$. Therefore, the expression of the demagnetization tensor depends on the permeability tensor field $\underline{\underline{\mu}}(\mathbf{x})$ in all points of the geometry, other than R_m. In our implementation of the optimization approach, the operator $\underline{\underline{N}}$ is never calculated explicitly. Rather, Eqs. (1) and (2) are coupled and solved for either the magnetic scalar potential or the magnetic vector potential. However, considering this operator is helpful in understanding the optimization method discussed here.

As also noted in other works employing the adjoint method [8,9], the key point is that the operator $\underline{\underline{N}}$ is a symmetric operator: this means that for each pair of vector fields $\mathbf{V}_1(\mathbf{x})$ and $\mathbf{V}_2(\mathbf{x})$ we have

$$\underline{\underline{N}} = \underline{\underline{N}}^T, \quad \text{i.e.,} \quad \int dV \mathbf{V}_1(\mathbf{x}) \cdot \left(\underline{\underline{N}}\mathbf{V}_2(\mathbf{x})\right)$$
$$= \int dV \left(\underline{\underline{N}}\mathbf{V}_1(\mathbf{x})\right) \cdot \mathbf{V}_2(\mathbf{x}). \tag{7}$$

This result is also referred to as the reciprocity theorem [14, 17], and, as we will see below, it plays a central role in our optimization approach. By considering the kernel $\underline{\underline{N}}(\mathbf{x}, \mathbf{x}')$, the theorem can also be expressed as $N_{ij}(\mathbf{x}, \mathbf{x}') = N_{ji}(\mathbf{x}', \mathbf{x})$. In the context of the adjoint method, it is expressed by saying that Poisson's equation, of which Eq. (5) is the formal solution, is self-adjoint [9].

We consider an objective functional $\mathcal{S} = \mathcal{S}[\mathbf{H}]$, which depends on the vector field $\mathbf{H}$. Denoting by $\mathbb{V}_g$ the set of all square-integrable vector fields $\mathbf{H} : (R_g \subset \mathbb{R}^3) \to \mathbb{R}^3$, then $\mathcal{S}$ is a functional $\mathcal{S} : \mathbb{V}_g \to \mathbb{R}$. Analogously, we will denote by $\mathbb{V}_m$ the set of all square-integrable vector fields over $R_m \subset \mathbb{R}^3$.

We now introduce the effective magnetization, which is a vector field over R_g defined as the gradient of $\mathcal{S}[\mathbf{H}]$ with

respect to $\mathbf{H}$:

$$\mathbf{M}_{\text{eff}}[\mathbf{H}^*] = (\nabla_{\mathbf{H}}\mathcal{S})_{\mathbf{H}^*}. \qquad (8)$$

This means that the $\mathbb{R}^3$ vector $\mathbf{M}_{\text{eff}}(\mathbf{x})$, where $\mathbf{x}$ is an arbitrary point in R_g, is the derivative of $\mathcal{S}$ with respect to the magnetic field at that point, i.e., with respect to $\mathbf{H}(\mathbf{x})$. With a loose notation, we can indicate this with the following equation:

$$\mathbf{M}_{\text{eff}}(\mathbf{x}) = \frac{\partial\mathcal{S}}{\partial\mathbf{H}(\mathbf{x})}. \qquad (9)$$

The left-hand side of Eq. (8) highlights the fact that, when considering the dependence on the starting point $\mathbf{H}^* \in \mathbb{V}_g$, the effective magnetization can be seen as a nonlinear operator $\mathbf{M}_{\text{eff}} : \mathbb{V}_g \to \mathbb{V}_g$, having $\mathbf{H}^*$ as input. The variation of $\mathcal{S}$ with respect to a variation $\delta\mathbf{H}$ is thus given by

$$(\delta\mathcal{S})_{\mathbf{H}^*} = \int_{R_g} dV\,\mathbf{M}_{\text{eff}}[\mathbf{H}^*] \cdot \delta\mathbf{H}. \qquad (10)$$

We also introduce the effective field, which is a vector field over R_m defined as the gradient of $\mathcal{S}[\mathbf{H} = \underline{\underline{N}}\mathbf{M}]$ with respect to $\mathbf{M}$. Applying the chain rule we get

$$\mathbf{H}_{\text{eff}}[\mathbf{M}^*] = (\nabla_{\mathbf{M}}\mathcal{S})_{\mathbf{M}^*} = \underline{\underline{N}}^T (\nabla_{\mathbf{H}}\mathcal{S})_{\underline{\underline{N}}\mathbf{M}^*} = \underline{\underline{N}}^T\mathbf{M}_{\text{eff}}[\underline{\underline{N}}\mathbf{M}^*]. \qquad (11)$$

The effective field $\mathbf{H}_{\text{eff}}$ in the point $\mathbf{x} \in R_m$ is thus the derivative of $\mathcal{S}$ with respect to the magnetization vector $\mathbf{M}(\mathbf{x})$ evaluated at that point:

$$\mathbf{H}_{\text{eff}}(\mathbf{x}) = \frac{\partial\mathcal{S}}{\partial\mathbf{M}(\mathbf{x})}. \qquad (12)$$

The effective field can also be seen as an operator $\mathbf{H}_{\text{eff}} : \mathbb{V}_m \to \mathbb{V}_m$ having $\mathbf{M}^*$ as input. The variation of $\mathcal{S}$ with respect to a variation $\delta\mathbf{M}$ is thus given by

$$(\delta\mathcal{S})_{\mathbf{M}^*} = \int_{R_m} dV\,\mathbf{H}_{\text{eff}}[\mathbf{M}^*] \cdot \delta\mathbf{M}. \qquad (13)$$

As we anticipated, the reciprocity theorem implies that the linear operator $\underline{\underline{N}}$ appearing in Eqs. (5) and (11) is a symmetric operator. Therefore, we can rewrite Eq. (11) as

$$\mathbf{H}_{\text{eff}}[\mathbf{M}^*] = \underline{\underline{N}}\mathbf{M}_{\text{eff}}[\underline{\underline{N}}\mathbf{M}^*]. \qquad (14)$$

The significance of the previous equation in relation to magnet design problems is that the derivative of $\mathcal{S}$ with respect to $\mathbf{M}$, i.e., the effective magnetic field, is the field generated by the effective magnetization. The key observation is that, even in circumstances where the closed
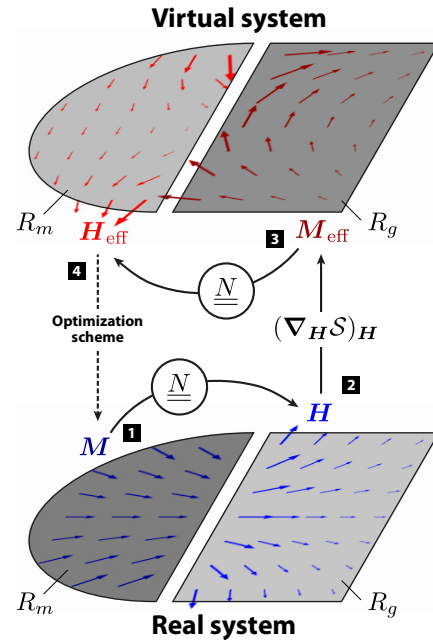

FIG. 1. Schematic illustration of the optimization approach. At each step of the optimization scheme discussed in Sec. II B, (1) the field is calculated from the current magnetization distribution: $\mathbf{H} = \underline{\underline{N}}\mathbf{M}$. Then (2) the effective magnetization is calculated from the current $\mathbf{H}$ vector field using the analytical expression of the gradient of $\mathcal{S}$ with respect to $\mathbf{H}$. Then (3) the effective field, which is the gradient of $\mathcal{S}$ with respect to the optimization variable $\mathbf{M}$, is computed as the field generated by the effective magnetization, i.e., $\mathbf{H}_{\text{eff}} = \underline{\underline{N}}\mathbf{M}_{\text{eff}}$. During the optimization scheme, $\mathbf{H}_{\text{eff}}$ is used to evolve the magnetization $\mathbf{M}$ towards the optimal solution (4).

form expression of $\underline{\underline{N}}$ is not known, the effective magnetization can still be calculated analytically for many relevant classes of objective functionals. The gradient-based approach that can be derived from this observation considerably reduces the computational complexity of the optimization problem. The optimization approach is schematically illustrated in Fig. 1. Appendix A 4 includes an introduction of the adjoint method, and highlights how the approach described here can be seen in that perspective.

Some of the assumptions stated at the beginning of this section were introduced only to make the explanation of the procedure more transparent, but are not necessary for the algorithm to work. For example, it should be noted that the whole optimization procedure would work in a very similar way if we assumed the remanent flux density $\mathbf{B}_{\text{rem}}$ as optimization variable, and $\mathbf{B} = \underline{\underline{\mu}}\mathbf{H} + \mathbf{B}_{\text{rem}}$ as constitutive relation in R_m; the permeability tensor $\underline{\underline{\mu}}$ would still be predetermined, i.e., not optimized. Moreover, we may have other sources of field within our geometry outside R_m, such as other magnets or electric currents, that are not optimization variables. When this is the case, we

replace Eq. (5) with $\mathbf{H} = \mathbf{H}_{\text{ext}} + \underline{\underline{N}}\mathbf{M}$. The definition of the effective magnetization remains the same, in the sense that $\mathbf{M}_{\text{eff}}$ is the gradient of $\mathcal{S}$ with respect to the total field: $\mathbf{M}_{\text{eff}} = \mathbf{M}_{\text{eff}}[\mathbf{H}_{\text{ext}} + \underline{\underline{N}}\mathbf{M}]$. Instead, when computing the effective field from the effective magnetization, these sources are not considered: $\mathbf{H}_{\text{eff}} = \underline{\underline{N}}\mathbf{M}_{\text{eff}}$.

B. Optimization scheme

We now introduce the optimization approach, which is based on the Landau-Lifshitz equation [18–20]. We prescribe that the magnetization $\mathbf{M}(\mathbf{x})$ over the region R_m will evolve according to the following equation of motion:

$$\frac{d}{dt}\mathbf{M} = \alpha\,\mathbf{M} \times \mathbf{M} \times \mathbf{H}_{\text{eff}}. \tag{15}$$

This can be seen as a gradient-descent scheme for maximizing or minimizing $\mathcal{S}$ while preserving the norm of $\mathbf{M}$ at each point [21,22]. The sign of the scalar parameter α determines whether the objective will be minimized or maximized. The time variable denoted by t in Eq. (15) has no physical meaning, it is the continuous analogous to the number of steps in an iterative optimization procedure.

This equation is suitable for our problem, since generally the norm of the magnetization vector is determined by the choice of permanent-magnet material, while the direction is the unknown optimization variable. The equilibrium solution is obtained when $\mathbf{M}$ is parallel to $\mathbf{H}_{\text{eff}}$ at any point. In this configuration, it is impossible to improve the objective with a smooth transformation of $\mathbf{M}(\mathbf{x})$ without violating the normalization constraint.

When applied to linear objective functionals, the algorithm proposed here reduces to the virtual magnet method discussed in Ref. [14] and Ref. [15]. It is in fact apparent that the effective field considered here is equivalent to the virtual field discussed in the aforementioned references. Analogously, the effective magnetization takes the role of the virtual magnetization. Here we used the terms effective field and effective magnetization to highlight the connection to the formalism of the Landau-Lifshitz equation.

For the case of linear objectives however, the effective field is constant. This means that for linear objectives no iteration or optimization scheme is necessary: the optimal direction of the magnetization in each point is simply aligned to the virtual field. This is not the case for the general optimization objectives considered here.

Our optimization framework is based on the Landau-Lifshitz equation, and we are also employing the same terminology encountered in micromagnetism. However, here we are describing a different physical situation. The magnetization in R_m is the optimization variable of our problem, determined entirely by the optimization objective $\mathcal{S}$. Outside R_m, the magnetization is determined by the linear constitutive relation expressed by Eq. (4). In contrast, the problem solved by micromagnetism is to find the magnetization field that minimizes the free-energy functional $\mathcal{G}[\mathbf{M}]$. This functional is defined from $\mathbf{M}$ based on the laws of physics, while the functional $\mathcal{S}$ considered here simply expresses a design-optimization problem. At the macroscopic scale considered here, the micromagnetic phenomena are only taken into account through the constitutive relations. This is the most-widely used assumption for optimizing macroscopic magnetic systems. For example, the norm of the magnetization is assumed to be equal to the remanent magnetization and not, as it is in micromagnetism, to the saturation magnetization. It would be interesting to also consider the problem of optimizing magnetic systems at the scale at which micromagnetic effects, such as domain-wall motion, are crucial. However, this would require a more advanced approach and the problem would be much more computationally intensive.

C. Implementation example

The optimization framework described above can easily be implemented in, e.g., a single COMSOL Multiphysics finite-element model [23]. Three physics nodes are required. Two of them are magnetic field interfaces, corresponding to the real and effective systems. In these nodes, the set of equations introduced in Sec. I B are solved. The space-dependent permeability field $\underline{\underline{\mu}}(\mathbf{x})$ should be the same in both systems, so for example the soft-iron parts are included in both systems.

Besides this, the real system has magnetization $\mathbf{M}$ defined over R_m, and the effective system has magnetization $\mathbf{M}_{\text{eff}}$ defined over R_g. The analytical expression of $\mathbf{M}_{\text{eff}}$ as a function of the magnetic field $\mathbf{H}$ is included in the model. The magnetic field computed in this interface is $\mathbf{H}_{\text{eff}}$.

The third physics node included in the COMSOL model is a coefficient form partial differential equation (PDE) that governs the time evolution of $\mathbf{M}$, according to Eq. (15). In fact, the COMSOL model includes a time-dependent study step, to compute the solution of this equation. However, since the effective magnetization depends on $\mathbf{H}$, it is necessary to initialize its value with an initial stationary study step. The magnetization $\mathbf{M}$ given for this initialization step is the starting configuration of the optimization procedure.

Additional details on the COMSOL implementation are discussed in Appendix A 1.

III. CONTINUOUS CASE: EXAMPLES

In the following sections, we will consider different examples of typical magnet design and optimization problems. The purpose is to illustrate the versatility and efficacy of our optimization approach with realistic prototypical optimization problem. However, for the examples, the

exact geometrical measures of the different fixed parts are not relevant, and will thus not be reported.

Unless otherwise specified when soft-iron parts are present within the geometry, these are modeled with isotropic relative permeability equal to 1000. The relative permeability is assumed to be equal to 1 elsewhere. The norm of the magnetization is set to $\mu_0 \|\mathbf{M}\| = 1$ T. These values are merely set for convenience, and the optimization scheme will work for all variables.

In all the figures, the magnetization direction will be indicated by the black arrows, while the magnetic flux density $\mathbf{B}$ is indicated by the color and by field lines.

A. Field-component squared

As a first example, we consider the problem of maximizing the air-gap volume integral of H_y^2. The corresponding objective functional $\mathcal{S}$ is quadratic with respect to $\mathbf{H}$:

$$\mathcal{S}[\mathbf{H}] = \int_{R_g} dV \, H_y^2(\mathbf{x}). \tag{16}$$

The corresponding effective magnetization is easily calculated from Eq. (8):

$$\mathbf{M}_{\text{eff}}(\mathbf{x}) = 2H_y(\mathbf{x})\hat{\mathbf{e}}_y. \tag{17}$$

Outside the air gap R_g the effective magnetization is zero. We apply this objective to the case of a rectangular magnet presenting a rectangular cavity, i.e., the air gap. The inner and outer corners of the hollow rectangle have been rounded. The result, shown in Fig. 2(b), confirms that the approach generates a solution with high air-gap volume average of H_y. The simulation has been initialized from the starting configuration shown in Fig. 2(a), given by $\mathbf{M}(x,y) = \hat{\mathbf{e}}_y \text{sign}(|y| - \ell_y)$, where ℓ_y is half the height of the region R_g in y direction. Compared to the starting configuration, the optimal solution improves the value of $\mathcal{S}$ by 192%.

Note that the air-gap region R_g has been slightly distanced from the central cavity by a thin border, which is shown in the figure. This expedient prevents numerical instabilities that may arise when the region R_g (where the optimization objective is defined) is directly adjacent to the magnet region R_m. We will use the same precaution in most of the examples discussed in the next sections.

B. Magnetic energy

A typical magnet design problem is to maximize or minimize the magnetic energy stored in the empty region of space R_g. This is expressed by the following objective
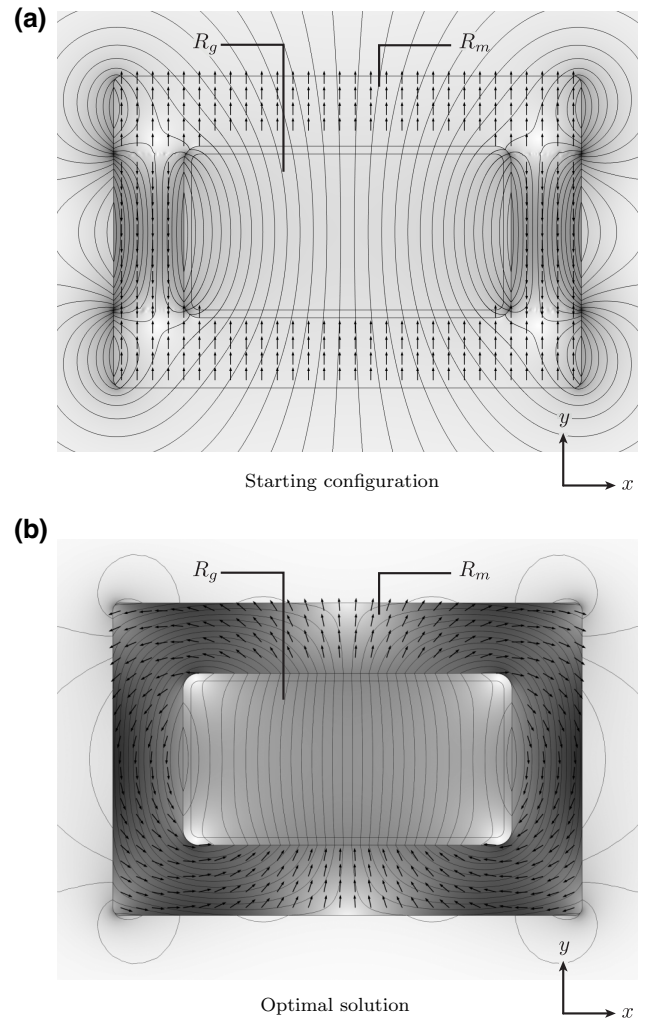

FIG. 2. The optimization objective is to maximize the integral over R_g of H_y^2. Figure 2(a) shows the starting configuration, and Fig. 2(b) the optimal solution. The value of the objective improves by 192%. As stated previously the magnetic flux density $\mathbf{B}$ is indicated by the color and by field lines.

functional:

$$\mathcal{S}[\mathbf{H}] = \int_{R_g} dV \, \|\mathbf{H}(\mathbf{x})\|^2. \tag{18}$$

The effective magnetization for this functional is again given by using Eq. (8), resulting in

$$\mathbf{M}_{\text{eff}}(\mathbf{x}) = 2\mathbf{H}(\mathbf{x}). \tag{19}$$

Minimizing the functional of Eq. (18) has the effect of insulating the region R_g from the field. The objective can also be applied to a subset of R_g to insulate only part of the air gap. The resulting objective functional would thus be similar to the one defined in Eq. (31). This strategy will be used in some of the examples presented in the next sections.

C. Field quality

Now we consider the problem of improving the field quality, with respect to any required distribution [24]. In particular, we assume a uniform vertical field as the target. It is insightful to think in terms of multipole expansions. The air-gap field $\mathbf{H}(\mathbf{x})$ shall be expanded into a series $\{\mathbf{u}_k(\mathbf{x})\}_{k=1,\ldots,\infty}$ of multipole fields, e.g., cylindrical harmonics, and we will denote with $\{c_k\}$ the coefficients of expansion:

$$\mathbf{H}(\mathbf{x}) = \sum_{k=1}^{\infty} c_k \mathbf{u}_k(\mathbf{x}). \tag{20}$$

We also assume that the first multipole component is the required air-gap field distribution. Our goal is to obtain a magnetic field distribution as close as possible to $\mathbf{u}_1(\mathbf{x})$ inside R_g. In other words, we wish to minimize the field distortion with respect to the required distribution. This goal can be expressed as the problem of minimizing the following objective functional:

$$\mathcal{S} = \sum_{k=2}^{\infty} |c_k|^2, \tag{21}$$

i.e., minimize all coefficients beside c_1. We assume that the various components of the expansion are orthonormal to each other:

$$\int_{R_g} dV \, \mathbf{u}_j(\mathbf{x}) \cdot \mathbf{u}_k(\mathbf{x}) = \delta_{jk}. \tag{22}$$

The coefficients of the expansion are thus given by

$$c_k = \int_{R_g} dV \, \mathbf{H}(\mathbf{x}) \cdot \mathbf{u}_k(\mathbf{x}). \tag{23}$$

Applying Parseval's identity [25] we obtain the following relation:

$$\int_{R_g} dV \, \|\mathbf{H}(\mathbf{x})\|^2 = \sum_{k=1}^{\infty} |c_k|^2 = |c_1|^2 + \sum_{k=2}^{\infty} |c_k|^2. \tag{24}$$

This allows us to write the objective $\mathcal{S}$ in a different form:

$$\mathcal{S} = \int_{R_g} dV \, \|\mathbf{H}(\mathbf{x})\|^2 - \left(\int_{R_g} dV \, \mathbf{H}(\mathbf{x}) \cdot \mathbf{u}_1(\mathbf{x}) \right)^2. \tag{25}$$

If $\mathbf{u}_1$ corresponds to a uniform field in the y direction that is normalized as required above, we have

$$\mathbf{u}_1(\mathbf{x}) = \left(\frac{1}{V_g} \right)^{1/2} \hat{\mathbf{e}}_y. \tag{26}$$

The objective is thus written as

$$\mathcal{S} = V_g \left(\langle H^2 \rangle_{R_g} - (\langle H_y \rangle_{R_g})^2 \right), \tag{27}$$

where V_g denotes the volume of R_g, and $\langle \ \rangle_{R_g}$ denotes the operation of taking the space average within R_g of the input argument.

Therefore, the effective magnetization becomes

$$\mathbf{M}_{\text{eff}}(\mathbf{x}) = 2\mathbf{H}(\mathbf{x}) - 2\hat{\mathbf{e}}_y \langle H_y \rangle_{R_g}. \tag{28}$$

We apply this objective to the same geometry considered in Fig. 2(b). However, due to the symmetry of the geometry, it is sufficient to simulate only one quarter of the geometry. At the boundary for which the field lines are parallel, i.e., the line $x = 0$, we apply a magnetic insulation boundary condition, i.e., $\hat{\mathbf{n}} \times \mathbf{A} = \mathbf{0}$ where $\hat{\mathbf{n}}$ is the unit vector normal to the surface and $\mathbf{A}$ is the magnetic vector potential; at the boundary for which the field lines are normal, i.e., the line $y = 0$ we apply a perfect magnetic conductor boundary condition, i.e., $\hat{\mathbf{n}} \times \mathbf{H} = \mathbf{0}$.

The results are shown in Fig. 3. The starting configuration used to initialize the algorithm is shown in Fig. 3(a). For the example shown in Fig. 3(b) the objective functional in the air gap is the one defined in Eq. (27). Additionally, for the example shown in Fig. 3(c), we require that in the region external to R_m the magnetic energy shall be minimized. As explained in Sec. III B this additional objective leads to a self-insulated magnet, as shown in Fig. 3(c). Both panels of Fig. 3 show that the intensity of the field in the air gap is on average lower than that of Fig. 2(b). However, for the examples of Fig. 3 the resulting field is perfectly homogeneous (up to the precision allowed by the numerical integration). By comparing Fig. 3(a) with Figs. 3(b) and 3(c), it is apparent that the optimization method successfully solved the problem.

We now consider the same optimization objective of the example shown in Fig. 3, but for a quadrupole field $\mathbf{u}_1(\mathbf{x})$ defined as

$$\mathbf{u}_1(\mathbf{x}) = \frac{y\hat{\mathbf{e}}_x + x\hat{\mathbf{e}}_y}{\left(\int_{R_g} dV \, y^2 + x^2 \right)^{1/2}}. \tag{29}$$

The effective magnetization is given by

$$\mathbf{M}_{\text{eff}}(\mathbf{x}) = 2\mathbf{H}(\mathbf{x}) - 2\mathbf{u}_1(\mathbf{x}) \left(\int_{R_g} dV' \, \mathbf{H}(\mathbf{x}') \cdot \mathbf{u}_1(\mathbf{x}') \right). \tag{30}$$

As geometry we consider a cylindrical magnet with a star-shaped cavity R_g located in its center. The result of the optimization is shown in Fig. 4. As can be seen, the approach was effective in calculating a magnetization distribution that generates a quadrupole field in the central
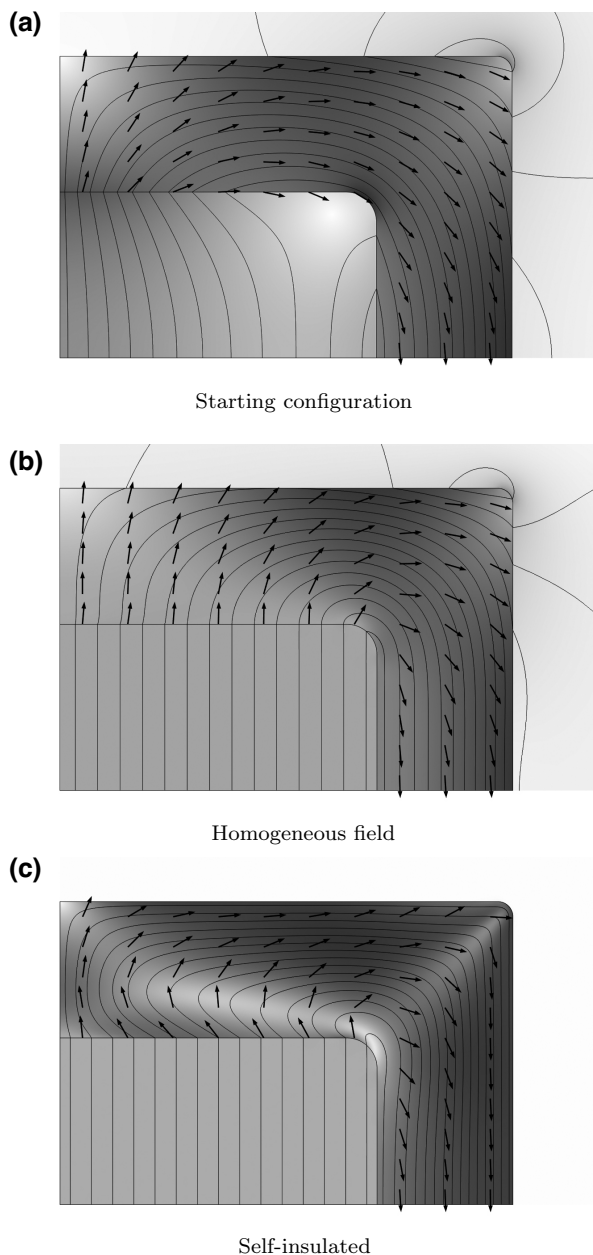
FIG. 3.   In this example the goal is to minimize the field distortion with respect to the required distribution, i.e., a uniform field oriented along the y direction. Figure 3(a) shows the starting configuration, and Fig. 3(b) shows the final result. For the example of Fig. 3(c) we additionally require that the magnetic flux leakage to the surrounding space is null.

cavity. Moreover, the magnet is perfectly self-insulated, as the flux leakage to the surrounding space is null.

The numerical results of the examples in Figs. 2(b), 3(b), and 3 are summarized in Table I. As we can see, the first case, which has been optimized for the objective of Eq. (16), gives a higher value for the three functionals listed in the rows of the table. However, the second and third case are also perfectly homogeneous, which is why the

values of the three functionals are the same. The lowest field strength corresponds to the case where we also require self-insulation.

D. Magnetic refrigeration

In this section we consider an example from magnetic refrigeration [26]. Here the air gap is composed of two adjacent empty regions R_{high} and R_{low}, such that $R_g = R_{\text{high}} \cup R_{\text{low}}$. The objective is to maximize and minimize the intensity of the field in R_{high} and R_{low}, respectively. This objective is expressed by the following functional:

$$
\mathcal{S}[\mathbf{H}] = \left(\frac{1}{V_{\text{high}}}\right) \int_{R_{\text{high}}} dV \, \|\mathbf{H}(\mathbf{x})\|^2
$$
$$
- \left(\frac{1}{V_{\text{low}}}\right) \int_{R_{\text{low}}} dV \, \|\mathbf{H}(\mathbf{x})\|^2. \quad (31)
$$

Therefore, the effective magnetization is given by

$$
\mathbf{M}_{\text{eff}}(\mathbf{x}) = + \left(\frac{2}{V_{\text{high}}}\right) \mathbf{H}(\mathbf{x}), \text{for } \mathbf{x} \in R_{\text{high}}
$$
$$
\mathbf{M}_{\text{eff}}(\mathbf{x}) = - \left(\frac{2}{V_{\text{low}}}\right) \mathbf{H}(\mathbf{x}), \text{for } \mathbf{x} \in R_{\text{low}} \quad (32)
$$

We apply this objective to a cylindrical geometry, as shown in Fig. 5. Here the air gap is the free region located between the central soft-iron core, and the external permanent-magnet region R_m. Only the first quadrant of the geometry is shown in Fig. 5, the remaining quadrants can be obtained by symmetry. As mentioned above, the air gap is subdivided into a high-field region and a low-field region. Each of these is composed of two 90° sectors located on opposite sides. North and south for the high-field region and east and west for the low-field region. One of the borders between the low- and high-field regions is shown in Fig. 5 as a dashed line. As seen from the figure, our approach led to a solution, which successfully focused the field into the high-field region, while diverting it from the low-field region.

E. Force between magnet and iron plane

We now consider the problem of maximizing the attractive force between a permanent magnet and a large soft-iron object. As illustrated in Fig. 6, we assume that the iron entirely occupies the region $y < 0$.

For this example we consider the limit $\mu_{\text{Iron}} \to +\infty$. In other words, $y = 0$ is the boundary of an infinite perfect magnetic conductor. This limit is obtained by applying the proper boundary condition at $y = 0$, while the region $y < 0$ is not actually part of the simulation. The magnet domain R_m is a rectangular prism located within the otherwise free
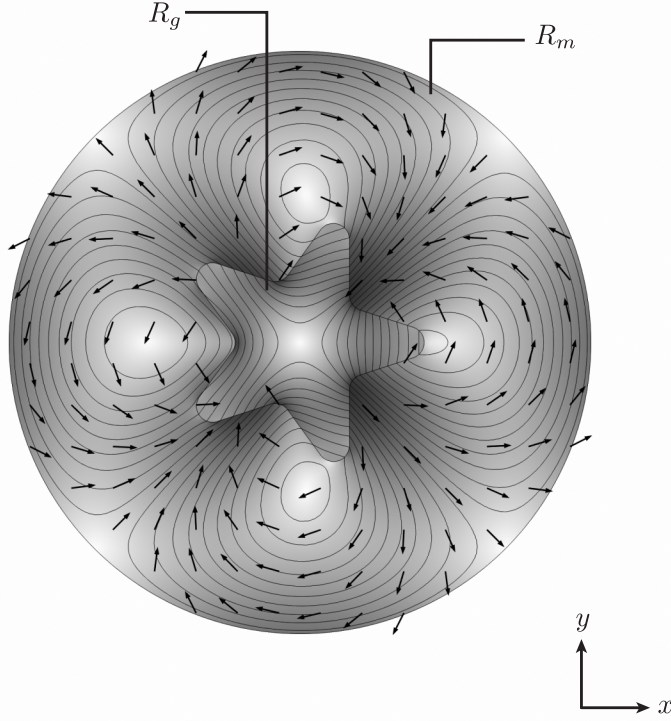
FIG. 4. In this example the goal is again to minimize the field distortion with respect to a required field distribution. However, here we require a quadrupole field in the central star-shaped cavity R_g. Additionally, we require self-insulation as for the example of Fig. 3(c).

region $y > 0$. The force acting on the magnet is computed from the Maxwell stress tensor $\underline{\underline{T}}$ [16]:

$$\mathbf{F} = \int_{\partial \Omega} dS \, \underline{\underline{T}} \, \hat{\mathbf{n}} \tag{33}$$

with

$$\underline{\underline{T}} = \left(\frac{1}{\mu_0}\right)\left(\mathbf{B}\mathbf{B}^T\right) - \underline{\underline{1}}\left(\frac{1}{2\mu_0}\right)\|\mathbf{B}\|^2. \tag{34}$$

The integration domain in Eq. (33) is the boundary $\partial\Omega$ of any region Ω that either encloses the magnet or encloses the iron object or separates them completely. It is thus convenient to chose an infinite plane parallel to the surface of the perfect conductor, and just outside of it, i.e., $y \to 0^+$. Being the surface located in air, we have $\mathbf{B} = \mu_0 \mathbf{H}$, which leads to

$$\underline{\underline{T}} = \mu_0\left(\mathbf{H}\mathbf{H}^T\right) - \underline{\underline{1}}\left(\frac{\mu_0}{2}\right)\|\mathbf{H}\|^2. \tag{35}$$

Since for our geometry $\hat{\mathbf{n}} \equiv \hat{\mathbf{e}}_y$, and $\mathbf{H}(\mathbf{x}) = H_y(\mathbf{x})\hat{\mathbf{e}}_y$, the only nonvanishing component of the force is the y component:

$$\mathbf{F} = \frac{\mu_0}{2}\int_{\partial\Omega} dS\,(H_y(\mathbf{x}))^2 \hat{\mathbf{e}}_y. \tag{36}$$

We thus assume the y component of the force as the optimization objective. For implementation reasons, our air-gap region shall be a very thin rectangle located at the boundary of the geometry, i.e., $y = 0^+$, and very long in the x direction, such that the magnetic field is nearly zero outside the left and right boundaries. The objective is then expressed as

$$\mathcal{S} = \mathbf{F} \cdot \hat{\mathbf{e}}_y = \frac{\mu_0}{2}\int_{R_g} dS\,(H_y(\mathbf{x}))^2 \tag{37}$$

and the effective magnetization is given by

$$\mathbf{M}_{\text{eff}}(\mathbf{x}) = \mu_0 H_y(\mathbf{x})\hat{\mathbf{e}}_y. \tag{38}$$

TABLE I. Different objectives associated to the goal of creating an air-gap field directed along the y direction. The corresponding solutions are shown in Figs. 2(b), 3(b), and 3(c), respectively. The starting cases 1 and 2 correspond to Figs. 2(a) and 3(a), respectively.

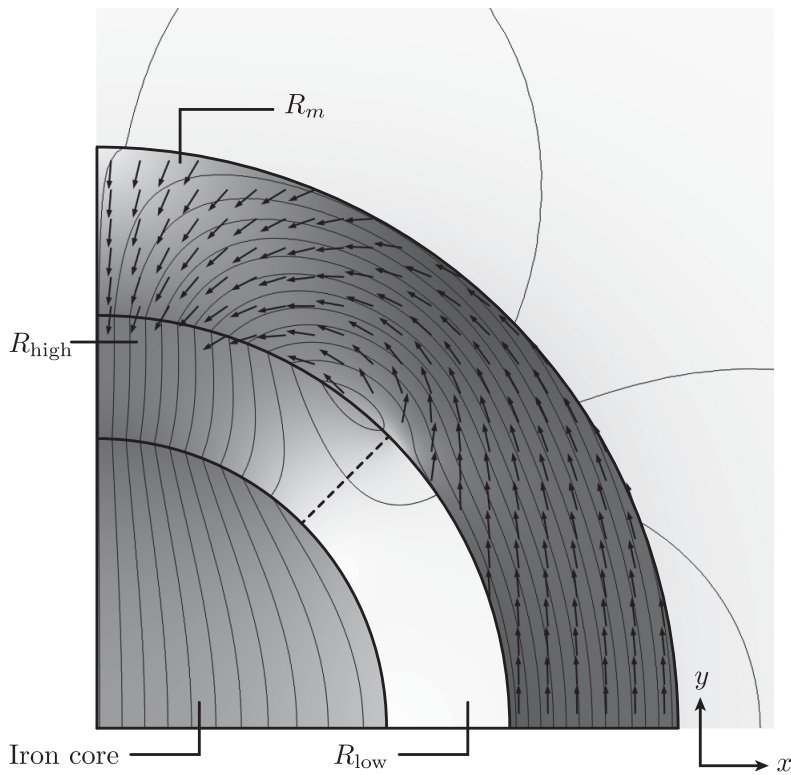|	Start 1	Start 2	Case 1	Case 2	Case 3
$V_g^{-1}\int dV\,\mu_0 H_y$	0.243 T	0.379 T	0.416 T	0.411 T	0.372 T
$\left(V_g^{-1}\int dV\,(\mu_0 H_y)^2\right)^{1/2}$	0.248 T	0.409 T	0.425 T	0.411 T	0.372 T
$\left(V_g^{-1}\int dV\,(\mu_0 H)^2\right)^{1/2}$	0.257 T	0.424 T	0.428 T	0.411 T	0.372 T

FIG. 5. This example is a rotary magnetic system applied to a magnetic refrigeration device. Here the goal is to maximize the square norm of the field within R_{high} and minimize it within R_{low}. Due to the symmetry, only one quarter of the geometry is shown.

We can notice the analogy between the expression of the objective $\mathcal{S}$ considered here with that considered in Sec. III A. The result shown in Fig. 6 has been optimized starting from a magnet uniformly magnetized in the positive y direction. Compared to the starting configuration, the objective improved by 135%.

F. Torque between magnetized cylinders

We consider two infinitely long co-axial cylinders, and assume cylindrical coordinates r, ϕ, and z, where the z axis lies on the common axis of the two cylinders. Our goal is to maximize the torque between the two cylinders. The z component of the torque $\boldsymbol{\tau}$ is given by [27]

$$\tau_z = \frac{1}{\mu_0} \int_0^{2\pi} d\phi \, r^2 B_r(\phi) B_\phi(\phi). \tag{39}$$

Let us assume that the magnetization distribution in one of the two cylinders, e.g., the inner cylinder, is known. For the illustrative example shown in Fig. 7, the inner cylinder is uniformly magnetized transversally to its axis. The relative rotation angle between the two cylinders is denoted by θ. We assume that the cylinder with known magnetization distribution is the one that is rotated by θ, while the cylinder with unknown magnetization distribution is stationary. The field generated by the rotating cylinder with known
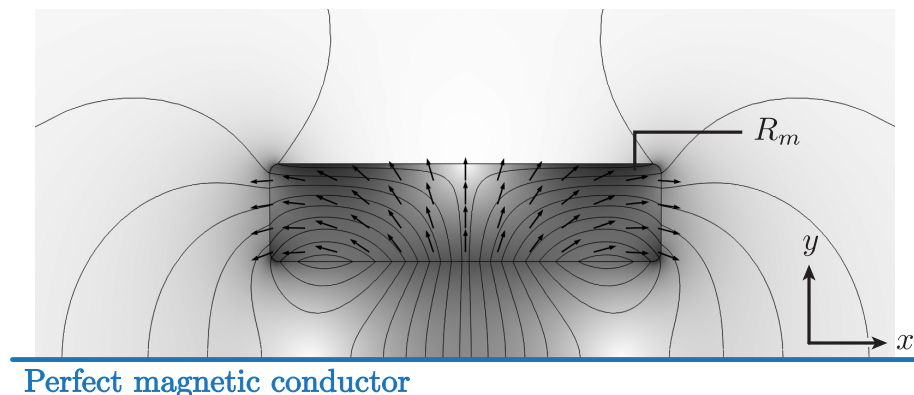

FIG. 6. For this case the objective is to maximize the attractive force between the permanent magnet R_m and the infinite iron part, which occupies the whole volume $y < 0$, where $y = 0$ corresponds to the thick blue line shown at the bottom of the figure. The iron part is modeled as a perfect magnetic conductor.
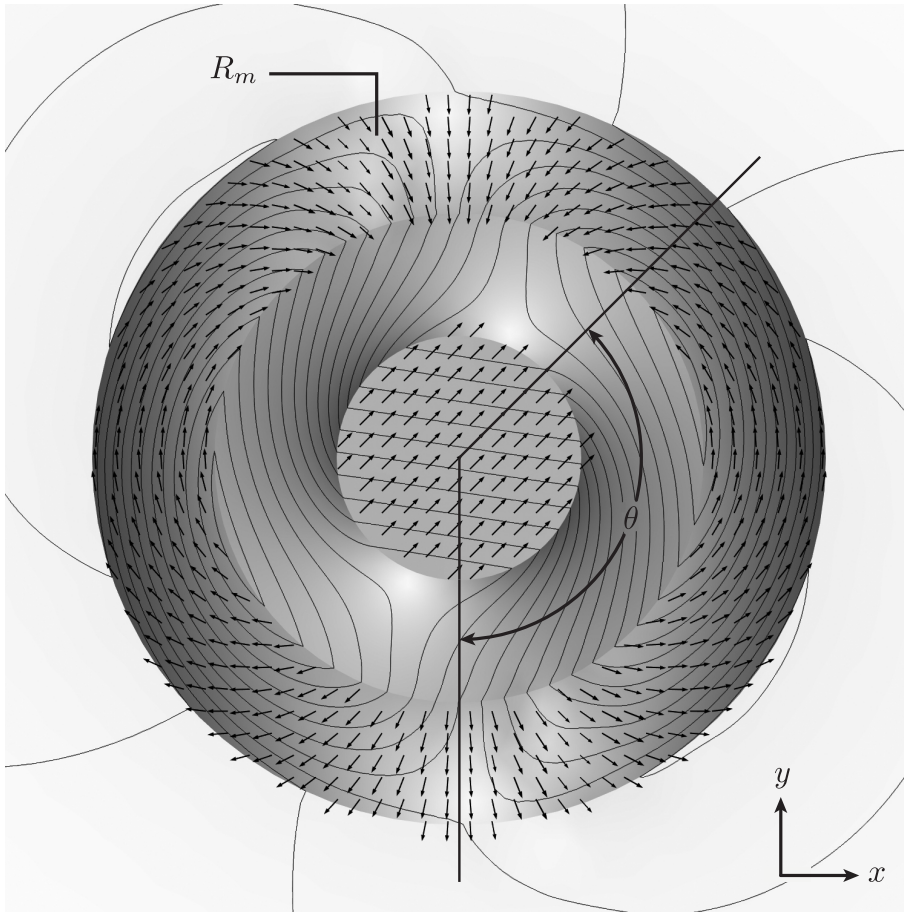
FIG. 7. The objective is to calculate the magnetization distribution within the external cylindrical permanent magnet such that it exerts the maximum torque over the central uniformly magnetized cylinder. Rather than optimizing the torque for a specific angular position θ, we maximize the mean square average of the torque over the full rotation $\theta \in [0, 2\pi]$. This objective is expressed by Eq. (43).

magnetization distribution will be denoted by

$$\mathbf{H}^{(\theta)}(\phi) = H_r^{(\theta)}(\phi)\hat{\mathbf{e}}_r + H_\phi^{(\theta)}(\phi)\hat{\mathbf{e}}_\phi. \qquad (40)$$

The total field is the sum of $\mathbf{H}^{(\theta)}$ with the field generated by the unknown magnetization of the external cylinder. The unknown field, (i.e., not the total field) is denoted by $\mathbf{H}$. Since in air $\mathbf{B} = \mu_0 \mathbf{H}$, the torque is given by

$$\tau_z(\theta) = \mu_0 \int_0^{2\pi} d\phi \, r^2 (H_r(\phi) + H_r^{(\theta)}(\phi))(H_\phi(\phi) \\ + H_\phi^{(\theta)}(\phi)). \qquad (41)$$

Should the objective have been $\tau_z(\theta)$ for fixed θ, the effective magnetization would have been obtained in the exact same way as described in the previous examples:

$$\tilde{\mathbf{M}}_{\text{eff}}^{(\theta)}(\phi) = r^2 \left((H_\phi(\phi) + H_\phi^{(\theta)}(\phi))\hat{\mathbf{e}}_r \\ + (H_r(\phi) + H_r^{(\theta)}(\phi))\hat{\mathbf{e}}_\phi \right). \qquad (42)$$

This objective would correspond to maximizing the instantaneous torque for a fixed rotation angle θ between the inner and the outer cylinders. However, a more relevant

objective is the mean square amplitude of the torque for $\theta \in [0, 2\pi]$.

$$\overline{\tau}_z = \frac{1}{2\pi} \int_0^{2\pi} d\theta \, (\tau_z(\theta))^2. \qquad (43)$$

Since the torque is quadratic, $\overline{\tau}_z$ clearly is not. The effective magnetization is given by

$$\mathbf{M}_{\text{eff}}(\phi) = \frac{1}{\pi} \int_0^{2\pi} d\theta \, \tau_z(\theta)\tilde{\mathbf{M}}_{\text{eff}}^{(\theta)}(\phi). \qquad (44)$$

We denote by $\mathbf{M}^{(\theta)}$ the (known) magnetization distribution that generates the field $\mathbf{H}^{(\theta)}$. This magnetization distribution must be included in the real system, but not in the virtual system.

The result, shown in Fig. 7, demonstrates that our approach can solve optimization problems even when the optimization objective has a relatively complicated dependence on the magnetic field. In fact, in this example the objective is obtained by averaging the torque over different relative positions between the inner and outer magnets.

G. Switch

In this section we consider a switchable field source, where the goal is to alternate between a high- and low-field states in the air gap [6]. For this purpose, we consider an objective functional, which depends on the field evaluated at two different configurations, corresponding to magnetic field distribution $\mathbf{H}_A$ and $\mathbf{H}_B$. The objective can be written as

$$\mathcal{S} = \mathcal{S}[\mathbf{H}_A, \mathbf{H}_B]. \tag{45}$$

For example, there could be a moving iron part, which assumes two different positions in the states "*A*" and "*B*." In this situation, we have two different states for the effective magnetization:

$$\mathbf{M}_{\text{eff}}^{(A)}[\mathbf{H}_A, \mathbf{H}_B] = \left(\nabla_{\mathbf{H}_A} \mathcal{S}\right)_{\mathbf{H}_A, \mathbf{H}_B}, \tag{46}$$

$$\mathbf{M}_{\text{eff}}^{(B)}[\mathbf{H}_A, \mathbf{H}_B] = \left(\nabla_{\mathbf{H}_B} \mathcal{S}\right)_{\mathbf{H}_A, \mathbf{H}_B}. \tag{47}$$

Since the position of the iron parts affects the permeability space dependence $\underline{\underline{\mu}}(\mathbf{x})$, the two configurations are characterized by different demagnetization tensors $\underline{\underline{N}}_A$ and $\underline{\underline{N}}_B$. The dependence of the objective on the magnetization $\mathbf{M}$ is thus written as

$$\mathcal{S}[\mathbf{M}] = \mathcal{S}[\underline{\underline{N}}_A \mathbf{M}, \underline{\underline{N}}_B \mathbf{M}]. \tag{48}$$

The effective field is thus given by

$$\mathbf{H}_{\text{eff}} = \underline{\underline{N}}_A \mathbf{M}_{\text{eff}}^{(A)} + \underline{\underline{N}}_B \mathbf{M}_{\text{eff}}^{(B)}. \tag{49}$$

For example, we could have an objective similar to the one for magnetic refrigeration:

$$mcS[\mathbf{H}] = \int_{R_g} dV \, \|\mathbf{H}_A(\mathbf{x})\|^2 - \int_{R_g} dV \, \|\mathbf{H}_B(\mathbf{x})\|^2. \tag{50}$$

This objective corresponds to the goal of maximizing the difference of the mean square amplitude of the field between the high-field state and the low-field state. The effective magnetization is thus given by

$$\mathbf{M}_{\text{eff}}^{(A)}(\mathbf{x}) = +2\mathbf{H}_A(\mathbf{x}), \tag{51}$$

$$\mathbf{M}_{\text{eff}}^{(B)}(\mathbf{x}) = -2\mathbf{H}_B(\mathbf{x}). \tag{52}$$

In the example shown in Fig. 8, the air-gap region R_g is the circular cavity in the center. The magnet design region R_m is the external permanently magnetized cylinder. Between R_g and R_m is a soft-iron structure occupying two opposite 90° angular sectors, i.e., the left and right sectors in Fig. 8(a), and the top and bottom sectors in Fig. 8(b). These positions correspond to the high-field and low-field states, respectively. Besides the optimization objective described above, for the example of Fig. 8 we also required that the structure is self-insulated in both states, such that the flux leakage to the surrounding space is minimized. This is done exactly in the same way discussed in Sec. III C. As seen in the figure, although the resulting self-insulation is not perfect in the low-field state of Fig. 8(b), the method did produce a satisfactory result.
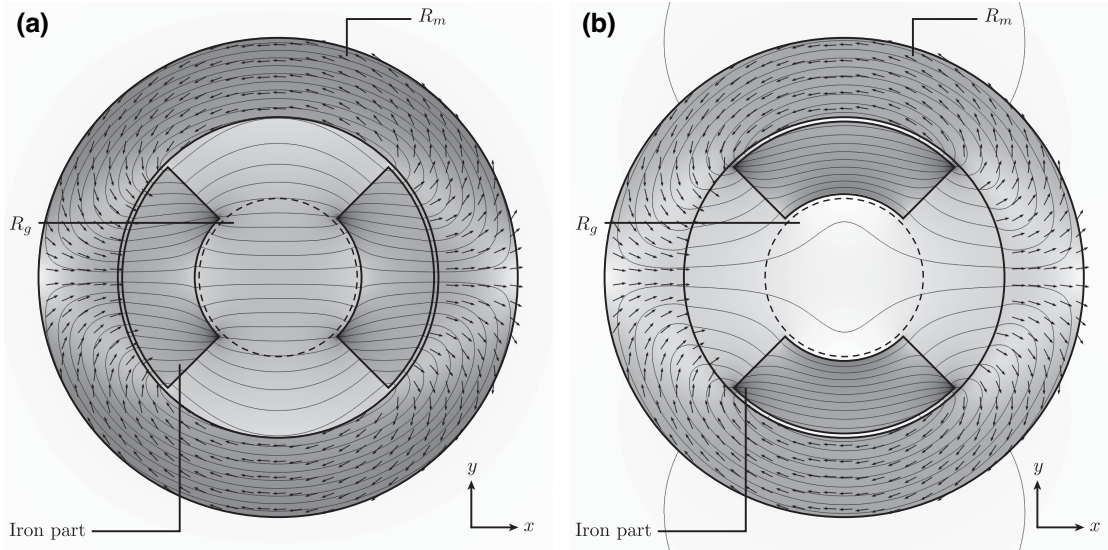

FIG. 8. In this example the goal is to optimize a switchable magnetic field source. The switching is performed by rotating the iron parts shown in the figure by 90°. The objective is thus to maximize the difference of the field-squared norm between the two states. Moreover, we require that the flux leakage to the surrounding space is minimized.
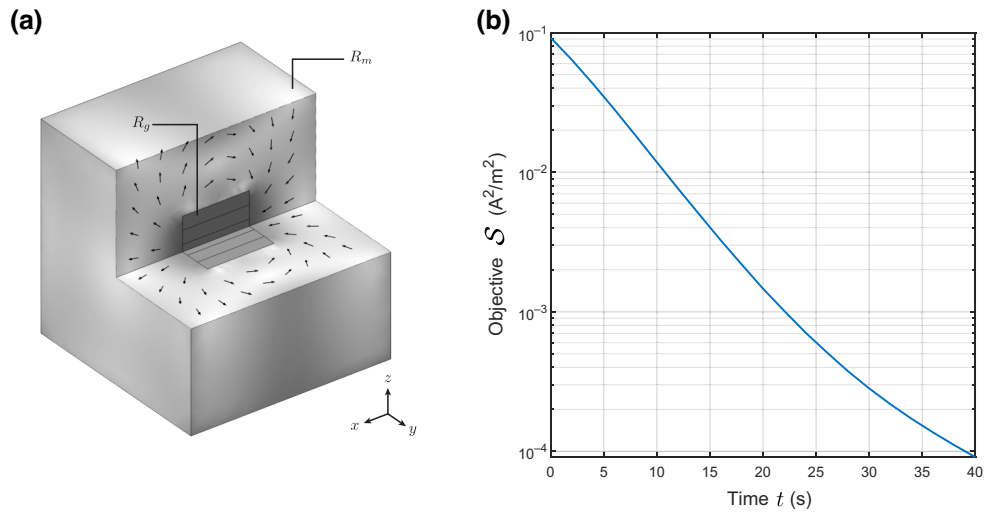
FIG. 9. The goal of this three-dimensional example is the same as for the case discussed in Sec. III C, namely to minimize the field distortion with respect to a uniform field directed along the x direction. Figure 9(a) shows the optimal solution, while Fig. 9(b) shows the evolution of the value of $\mathcal{S}$ during the optimization procedure; here the variable denoted as "time" indicates how long has the optimization been carried for. As can be seen, the field distortion is reduced by 3 orders of magnitude.

H. Three-dimensional rectangular cavity

Our optimization approach can be employed for three-dimensional optimization problems as well. To demonstrate its effectiveness, we study the same optimization objective discussed in Sec. III C, i.e., minimizing the field distortion with respect to a required field distribution. In particular, we consider the following objective functional, which is analogous to that expressed by Eq. (27):

$$\mathcal{S} = \left(\langle H^2 \rangle_{R_g} - (\langle H_x \rangle_{R_g})^2 \right). \qquad (53)$$

The goal is thus to generate in R_g a perfectly uniform field oriented in the x direction. The geometry, shown in Fig. 9(a), consists of a permanent-magnet cube with a central cubic cavity R_g. As can be seen from the field lines shown in R_g, the resulting magnetic field is indeed homogeneous within the air gap.

The starting configuration used for this problem has **M** aligned to the field generated by a point magnetic dipole located in the center of the air gap, and oriented along the x direction. Figure 9(b) shows the evolution of the value of $\mathcal{S}$ as the optimization progresses according to Eq. (15). The simulation has been carried out until the field distortion is reduced by 3 orders of magnitude with respect to the starting configuration. As can be seen, the objective could have improved even more if the optimization had been continued for a longer time span. As for the examples discussed in Sec. III C, the limit is the precision allowed by the approximations that are always present when performing any numerical computation.

IV. SEGMENTED MAGNETIZATION CASE

A. Introduction

In this section we will focus on permanent-magnet systems that are segmented into a given number N of uniformly magnetized pieces. The optimization objective will be formulated exactly as for the continuous case. The problem is then to determine the optimal set of N regions occupied by the pieces and the directions of the corresponding N magnetization vectors. The norm of the magnetization is again assumed to have fixed value in R_m.

As we will see, for segmented systems we have two sufficient conditions for the solution to be optimal with respect to the considered objective. One condition will apply to the set of regions and the other one to the magnetization vectors. These optimality conditions are analogous to those discussed in Ref. [15] for the case of linear objectives. However, for the nonlinear case these conditions have a purely local value as they are based on the effective field $\mathbf{H}_{\text{eff}} = (\nabla_{\mathbf{M}} \mathcal{S})_{\mathbf{M}}$, which is the gradient of a nonlinear objective and as such depends on the point $\mathbf{M}$ at which it is evaluated. Therefore, while it is possible to calculate the infinitesimal transformation to the regions or the magnetization vectors that will result in the largest variation of $\mathcal{S}$, there is no way to perform a finite transformation guaranteed to improve the value of $\mathcal{S}$. Nevertheless, the two sufficient conditions for an optimal solution form the basis upon which an efficient optimization algorithm can be built.

Let us now consider how the two conditions can be derived for the case of a general nonlinear objective. The starting observation is that as long as we transform the current magnetization distribution $\mathbf{M}_0$ by an infinitesimal

variation $\delta\mathbf{M}$, the variation of the objective $\mathcal{S}$ can be computed with the linear approximation:

$$\delta\mathcal{S} = \int_{R_m} dV\, (\mathbf{H}_{\text{eff}}[\mathbf{M}_0]) \cdot \delta\mathbf{M}. \qquad (54)$$

In other words, the variation $\delta\mathcal{S}$ is computed from the variation $\delta\mathbf{M}$ multiplied by the gradient of $\mathcal{S}$ evaluated at the starting point $\mathbf{M}_0$: the gradient $\mathbf{H}_{\text{eff}}$ is thus assumed fixed.

Such an assumption is valid as long as the functional $\mathcal{S}$ is continuous [25] with respect to the adopted Hilbert space norm $\|\cdot\|_H$

$$|\mathcal{S}[\mathbf{M}_0 + \delta\mathbf{M}] - \mathcal{S}[\mathbf{M}_0]| \to 0, \quad \text{if } \|\delta\mathbf{M}\|_H \to 0. \quad (55)$$

As norm, we will consider the square integral over R_m:

$$\|\delta\mathbf{M}\|_H = \left(\int_{R_m} dV\, \|\delta\mathbf{M}(\mathbf{x})\|^2\right)^{1/2}. \qquad (56)$$

Let us consider the following variation:

$$\delta\mathbf{M}_1 = \lim_{m(R)\to 0} \begin{cases} \mathbf{\Delta}, & \text{for } \mathbf{x} \in R \\ \mathbf{0}, & \text{for } \mathbf{x} \notin R \end{cases}, \qquad (57)$$

with $\|\mathbf{\Delta}\| > 0$. Here $R \subset R_m$ denotes a region of space, $m(R)$ denotes the volume of R, and $\mathbf{\Delta}$ denotes a vector $\in \mathbb{R}^3$. The variation corresponds to transforming $\mathbf{M}(\mathbf{x})$ by a finite amount $\mathbf{\Delta}$, but over an infinitesimally small region of space R.

One can think of the opposite situation where the magnetization of a finite region is transformed by an infinitesimal amount, which corresponds to the following variation:

$$\delta\mathbf{M}_2 = \lim_{\|\Delta\|\to 0} \begin{cases} \mathbf{\Delta}, & \text{for } \mathbf{x} \in R \\ \mathbf{0}, & \text{for } \mathbf{x} \notin R \end{cases}, \qquad (58)$$

with $m(R) > 0$.

Both the variations $\delta\mathbf{M}_1$ and $\delta\mathbf{M}_2$ satisfy $\|\delta\mathbf{M}\|_H \to 0$, with the Hilbert-space norm defined in Eq. (56). In fact for $\delta\mathbf{M}_1$ we have

$$\|\delta\mathbf{M}_1\|_H = \|\mathbf{\Delta}\| \lim_{m(R)\to 0} m(R)^{1/2} = 0 \qquad (59)$$

and for $\delta\mathbf{M}_2$ we have

$$\|\delta\mathbf{M}_2\|_H = m(R)^{1/2} \lim_{\|\Delta\|\to 0} \|\mathbf{\Delta}\| = 0. \qquad (60)$$

A continuous functional would give an infinitesimal variation $\delta\mathcal{S}$ for each of the two variations $\delta\mathbf{M}_1$ and $\delta\mathbf{M}_2$. All the objective functionals considered in this work satisfy the continuity condition. Two counterexamples of noncontinuous functionals are given in Appendix A 2.

In the following sections we will use the variations $\delta\mathbf{M}_1$ and $\delta\mathbf{M}_2$ to construct the two optimality conditions for nonlinear continuous objectives. It should be stressed that the relevance of these conditions goes beyond the iterative optimization approach that we employed in this work. In fact, regardless of the method used to design a segmented magnetic system, if it is optimal for a given optimization objective it must necessarily obey those conditions. These can thus be used as a test to evaluate the optimality of any magnetic system with respect to any optimization objective that can be expressed as $\mathcal{S}[\mathbf{H}]$.

B. Optimal regions

We assume that the set of magnetization vectors of the segments is fixed, and the set of regions is locally optimal. *Then on each point of the boundary between two adjacent segments, the effective field is equally aligned (i.e., it gives the same scalar product) with the magnetization vectors of the two segments.*

This can be seen by assuming that the condition above is not verified and considering a suitable infinitesimal variation $\delta\mathbf{M}_1$. If at any point on the boundary the magnetization vectors are not equally aligned to $\mathbf{H}_{\text{eff}}$, it would be convenient to reassign that point to the region giving the best alignment. Such an infinitesimal transformation corresponds to a variation $\delta\mathbf{M}_1$ of the kind defined by Eq. (57). As seen from Eq. (54), such a variation would increase the value of $\mathcal{S}$, and therefore the starting configuration could not have been optimal.

C. Optimal directions

We assume that the set of regions is fixed, and the set of magnetization vectors of the segments is locally optimal. *Then the cross product between the magnetization vector of each segment and the average effective field over the corresponding region is zero, i.e., they are parallel to each other.*

Again, we can assume that the condition is not verified and consider a suitable variation $\delta\mathbf{M}_2$. In this case we rotate by an infinitesimal amount the magnetization vector over the whole region occupied by one of the segments. This corresponds to a variation $\delta\mathbf{M}_2$ such as those defined in Eq. (58). As seen from Eq. (54), if the magnetization vector of the region is not initially aligned to the average effective field, the value of $\mathcal{S}$ could be increased by an infinitesimal rotation towards the average of $\mathbf{H}_{\text{eff}}$ over the region. This argument shows that the initial configuration could not have been optimal.

D. Iterative optimization procedure

We consider an iterative optimization procedure based on the optimality conditions discussed in the previous sections. The procedure starts with an initial guess of the N

uniformly magnetized regions $\{R_n\}_{n=1,...,N}$ and the corresponding N magnetization vectors $\{\mathbf{M}_n\}_{n=1,...,N}$. From the resulting magnetization field $\mathbf{M}$ we compute the field $\mathbf{H}$ generated by it. Then we compute the effective magnetization and the effective field generated by it. These vector fields are all used to initialize the iteration. Each step of the iteration consists of the following sequence of substeps:

(1) **Updating the regions:** the N uniformly magnetized regions are updated. We consider the set $R(0) \subset R_m$ of all the points $\mathbf{x}$ where a better alignment between $\mathbf{H}_{\text{eff}}$ and $\mathbf{M}_n$ could be achieved by reassigning $\mathbf{x}$ to a different uniformly magnetized region other than the current one. A portion of the total volume of this set is reassigned, each point to the region giving the best alignment. The control parameter $\alpha_{\text{reg.}}$ corresponds to the volume of the reassigned region normalized by the volume of $R(0)$.

(2) **Computing the effective field:** the effective field is recomputed according to the updated regions.

(3) **Updating the directions:** the magnetization vectors of the N regions are updated. For each of the N uniformly magnetized regions, we consider the angle θ_n^* between the corresponding magnetization vector $\mathbf{M}_n$ and the average of the effective field over that region. The magnetization vectors are rotated towards the average effective field by a fraction of the angle θ_n^*. The control parameter $\alpha_{\text{dir.}}$ corresponds the angle of this rotation region normalized by the maximum angle θ_n^*.

(4) **Computing the effective field:** the effective field is recomputed according to the updated directions.

As long as the variations performed in steps 1 and 3 are sufficiently small, then the associated variation of the objective $\mathcal{S}$ is accurately described by Eq. (54). When this is true, the procedure is guaranteed to lead to a monotonic increase of $\mathcal{S}$. The iteration is interrupted when the variation of $\mathcal{S}$ between two consecutive steps is below a certain threshold.

Note that when $\alpha_{\text{reg.}}$ and $\alpha_{\text{dir.}}$ are both set to 0, the regions and directions do not evolve at all; the infinitesimal variation case $\|\delta\mathbf{M}\|_H \to 0$ is found close to this limit. Vice versa, when $\alpha_{\text{reg.}}$ and $\alpha_{\text{dir.}}$ are both set to 1, the variation is maximal. In this situation, the algorithm corresponds to the Lloyd iteration described in Ref. [15], except that the effective field is recomputed every time either the regions or the directions are updated.

E. Implementation

Our implementation uses COMSOL Multiphysics with MATLAB. Steps 2 and 4 where the effective field is recomputed are performed within the two COMSOL magnetic field interfaces mentioned in Sec. II C. Steps 1 and 3, i.e., updating the uniformly magnetized regions and the corresponding magnetization vectors, are performed within MATLAB

and the results are passed back to COMSOL. Appendix A 3 includes additional details on the implementation of steps 1 and 3.

V. SEGMENTED CASE: EXAMPLES

All the assumptions and notations described at the beginning of Sec. III also apply to the segmented examples discussed in the next sections. Additionally, we set the values of both parameters $\alpha_{\text{reg.}}$ and $\alpha_{\text{dir.}}$ to 1, which corresponds to the maximal variation. Despite this, the iterations still resulted in monotonically increasing $\mathcal{S}$ and converged to an optimal solution for all the considered examples. This point is also discussed in Sec. VI.

A. Field intensity

In this example we consider the same geometry of the example discussed in Sec. III A, i.e., a rectangular magnet presenting a rectangular cavity. The goal is to generate inside the cavity a magnetic field directed vertically, i.e., along the y component. However, there is more than one objective functional that could be suitable for this goal. In particular, we consider three different possibilities. The first is the linear case, where the objective is expressed by the following functional:

$$\mathcal{S}_1 = \int_{R_g} dV \mu_0 H_y. \tag{61}$$

The second possibility is the root mean square of the y component of the field, i.e.,

$$\mathcal{S}_2 = \left(\int_{R_g} dV (\mu_0 H_y)^2 \right)^{1/2}. \tag{62}$$

Except for the 1/2 exponent, which does not cause any difference in the final result, this objective is identical to that discussed in Sec. III A.

Finally, we consider the problem of maximizing the air-gap magnetic energy, similar to the example of Sec. III B, i.e.,

$$\mathcal{S}_3 = \left(\int_{R_g} dV (\mu_0 H)^2 \right)^{1/2}. \tag{63}$$

However, since we would still like the field to be generally oriented in the y direction, we choose the starting configuration shown in Fig. 10(a) that will promote the desired solution.

The results for the three optimization objectives are shown in Figs. 10(b), 10(c), and 10(d), respectively. The numerical results for the starting configuration and the three cases are presented in the three columns of Table II. The different objectives are evaluated for all cases in
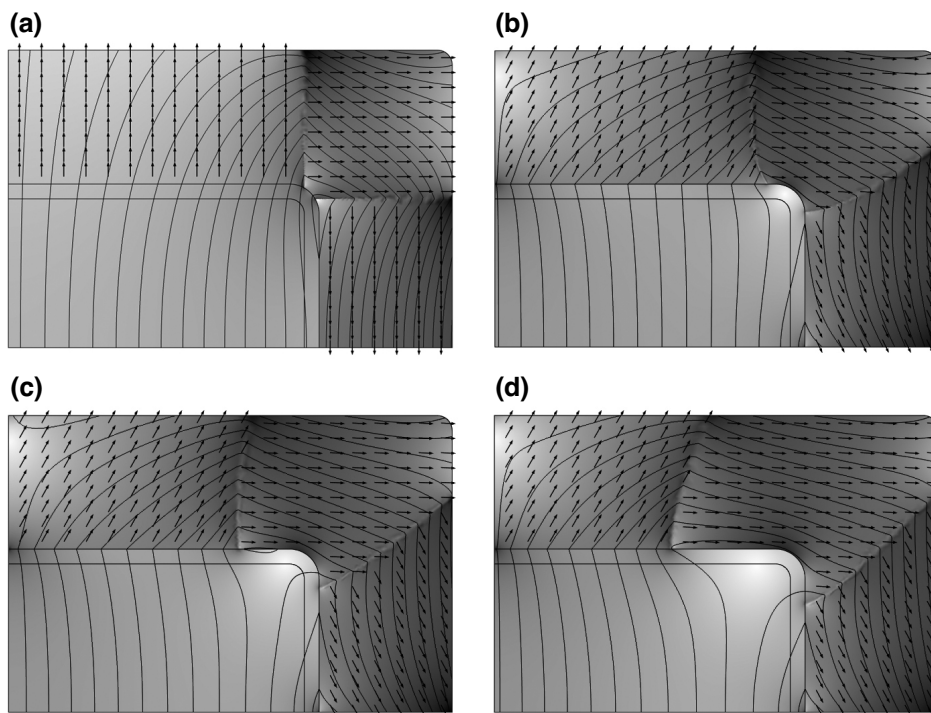
FIG. 10. In the three examples of Figs. 10(b), 10(c), and 10(d) the objective is to maximize the field intensity along the *y* direction. However, we can attain this goal by considering three different objective functionals, which are shown in Eqs. (61), (62), and (63), respectively. The starting state for all three cases is shown in Fig. 10(a). The geometry consists of a rectangular magnet with a central rectangular cavity, but only one quarter of the geometry is shown here. The numerical results are presented in Table II. Please note that none of these three examples has been optimized for self-insulation: the flux leakage outside R_m is simply not shown in these pictures.

the three rows of the table. However, the objective actually used during the optimization procedure is highlighted by bold font weight. As can be seen, each of the three functionals gives the maximum value for the corresponding case, which is a confirmation that the optimization approach is working correctly. In all cases, the value of the objective increased with respect to the starting configuration. These results can be compared with the analogous results for the continuous case, summarized in Table I. As can be seen, the continuous case optimized for the average of H_y^2 outperforms all the segmented cases, which is not surprising.

B. Force between magnet and iron plane

In this section we consider an optimization problem analogous to that discussed in Sec. III E. The objective is to realize a segmented permanent-magnet assembly that will exert the maximum force over a large iron plane located at some distance from the magnet. The only difference with respect to the discussion presented in Sec. III E is that here we apply the optimal segmentation procedure, with three segments. The result, shown in Fig. 11, demonstrates that the approach described in Sec. IV D is effective in computing optimally segmented magnetic assemblies for a wide variety of optimization objectives. In the next section we will elaborate the scope and limitations of the optimization approach for segmented assemblies.

VI. DISCUSSION

It is worth highlighting another fundamental difference between linear problems and nonlinear ones. This difference is related to the presence of a point-wise constraint on the norm of **M**, expressed as $\|\mathbf{M}(\mathbf{x})\| = M_0, \forall \mathbf{x} \in R_m$.

For a linear objective functional the derivative does not depend on the magnetization distribution. This property implies that, if the point-wise constraint on the norm of

TABLE II. Different objectives associated to the goal of creating an air-gap field directed along the *y* direction and maximize its intensity. The corresponding solutions are shown in Fig. 10.

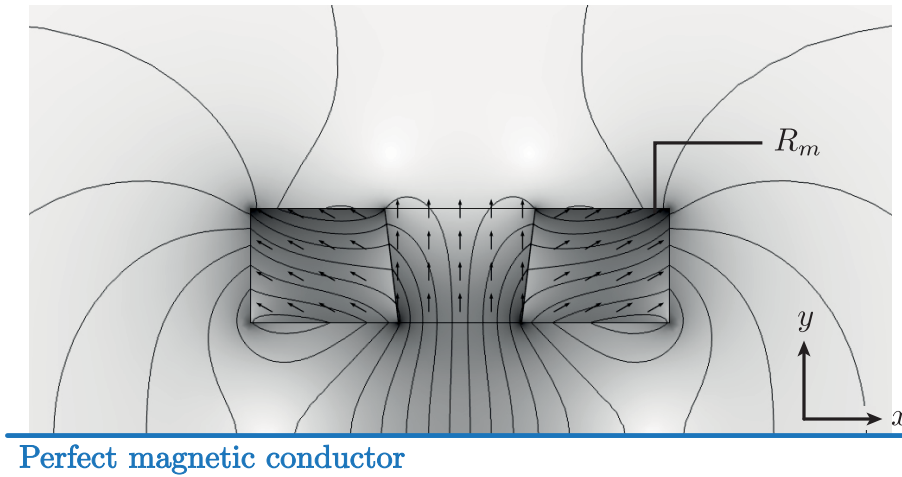|	Start	Case 1	Case 2	Case 3
$V_g^{-1} \int dV \, \mu_0 H_y$	0.357 T	**0.403 T**	0.400 T	0.388 T
$\left(V_g^{-1} \int dV \, (\mu_0 H_y)^2\right)^{1/2}$	0.361 T	0.405 T	**0.407 T**	0.404 T
$\left(V_g^{-1} \int dV \, (\mu_0 H)^2\right)^{1/2}$	0.362 T	0.407 T	0.410 T	**0.412 T**

FIG. 11. This example is analogous to that shown in Fig. 6, except that we consider the segmented solution. The goal is thus to maximize the attractive force between the rectangular permanent magnet and a large iron block, whose upper boundary is indicated by the blue line shown at the bottom of the figure.

M is not considered, there are no true equilibrium configurations. The optimal solutions would be "at infinity." For any magnetization configuration with finite norm, it would always be possible to improve the value of $\mathcal{S}$ by increasing the magnetization in the direction of the effective field. However, doing so would violate the constraint on the norm of **M**. Instead, if the constraint is applied, once the magnetization is aligned with the effective field everywhere, the configuration is at least locally optimal. This category of optimization problem is schematically illustrated in Fig. 12(a). This situation can also occur in some cases for nonlinear objectives, as for the example of maximizing the magnetic energy discussed in Sec. III B.

However, for nonlinear objectives this is not the only possible scenario. There could be an optimal solution of the constrained problem, which is simultaneously an optimal solution for the unconstrained problem, as illustrated in Fig. 12(b). In this scenario, for a locally optimal magnetization distribution **M** satisfying the constraint, the effective field is not just parallel to **M** everywhere, but it is zero at every point. This happens because the effective magnetization, i.e., the gradient of $\mathcal{S}$ with respect to **H**, is also zero at an equilibrium state of the unconstrained problem. This is, e.g., the case of the ideal Halbach cylinder with field homogeneity as objective, since the field is indeed perfectly homogeneous. This example is discussed in detail
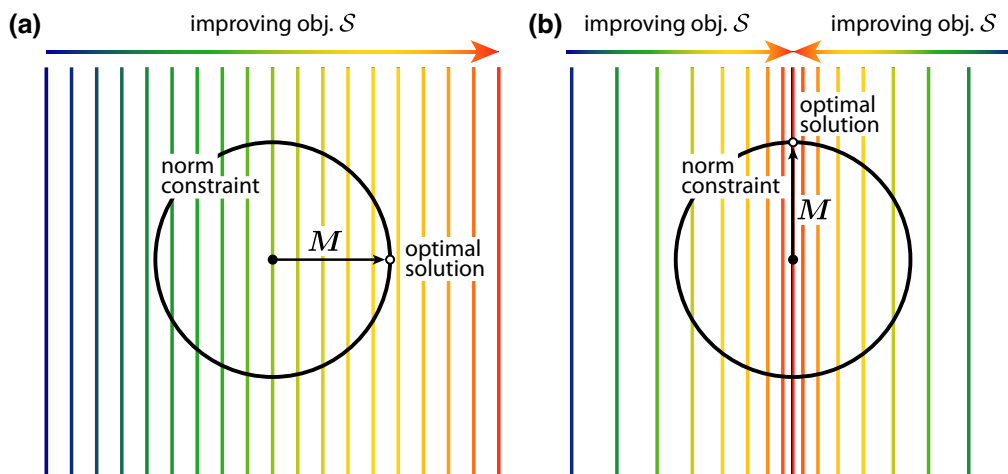

FIG. 12. Illustration of the two kinds of optimization problems. Figure 12(a) shows the category for which the optimal solution of the unconstrained problem is at infinity. Figure 12(b) shows the category for which there is an optimal solution of the unconstrained problem that is also compatible with the point-wise constraint. These plots show the magnetization vector in a single point of R_m for illustrative purpose. The arrows on the top of the figures show the direction in which the objective $\mathcal{S}$ is improving.

in Sec. III C. Clearly, if there is a magnetization distribution with uniform norm, which generates a perfectly homogeneous field, we can rescale the norm of the magnetization everywhere by the same factor and we would still get a perfectly homogeneous field. The same magnetization distribution would thus be a locally optimal point even without the constraint on the norm of **M**. Not only $\mathbf{M} \times \mathbf{H}_{\text{eff}}$ is zero everywhere, but the effective field itself is identically zero. When approaching such an equilibrium point, the magnitude of the effective field becomes smaller and smaller.

Neither of the two situations guarantees that the locally optimal configuration is also globally optimal. Although in some cases additional considerations might prove global optimality. For the example of the Halbach cylinder the field is perfectly homogeneous and $\mathcal{S} = 0$. Since $\mathcal{S}$ is always ≥ 0 this configuration is the globally optimal solution (although there might be different configurations also leading to $\mathcal{S} = 0$).

Among the examples that we considered, the second category of optimization objectives has been computationally harder to solve. This means that the optimal solution can in some circumstances be more significantly affected by the initial configuration. Moreover, the solver that integrates the equation of motion, Eq. (15), uses a greater number of time steps to achieve the desired tolerance. In fact, problems belonging to this category have proved to be difficult to solve for the segmented case. Therefore, we did not include any segmented examples of this case. However, our experiments indicate that it would be possible to solve similar problems with our approach, by tuning the values of the parameters $\alpha_{\text{reg.}}$ and $\alpha_{\text{dir.}}$. Instead, for the first category of optimization objectives, we obtained the desired results simply by setting these parameters to 1. This is an indication that even when performing relatively large variation of the magnetization distribution, the variation of the gradient of $\mathcal{S}$ is not so large as to render the gradient-based method ineffective.

VII. CONCLUSION

We discussed a gradient-based optimization approach based on the Landau-Lifshitz equation that can be applied to any nonlinear objective functional as long as the analytical expression of its derivative with respect to the magnetic field can be calculated.

The method assumes that a linear constitutive **B-H** relation is satisfied at any point, an assumption that is justified in a wide range of relevant magnet-design problems. The output is the magnetization distribution within the permanent-magnet material satisfying a point-wise constraint on the norm. We applied this constraint because the magnitude of the magnetization is determined by the choice of permanent-magnet material, while the direction of the magnetization is the actual unknown design variable.

Our key observation is that, when applying this constraint, the gradient-based optimization scheme reduces to the Landau-Lifshitz equation governing the evolution of the magnetization distribution over the magnet region. The linear constitutive relation, and the fact that the derivative of the objective is calculated analytically, ensure that the optimization algorithm is computationally efficient.

In fact, the underlying optimization problem is significantly easier to solve than the more general problem assumed by topology optimization approaches, because in our method we assume $\underline{\underline{\mu}}$ to be fixed and the **B-H** relation to be linear. By considering this less-general optimization problem we can apply a gradient-based approach which is more robust and computationally efficient than topology optimization. Despite being less general, the optimization problem solved by our approach is still very relevant for magnet-design applications, as we demonstrated by the many examples presented in our study.

We also discussed how a similar procedure can be applied to magnetic assemblies that are segmented into uniformly magnetized pieces. We observed that for some choices of optimization objective it can be problematic to solve the segmented optimization problem. Nonetheless, the different examples of segmented systems presented in our study indicate that the approach is an effective way of computing the optimal segmentation of magnetic systems for various relevant optimization objectives.

ACKNOWLEDGMENTS

APPENDIX

1. Building a COMSOL model

As mentioned in Sec. II C, for the continuous case our approach can be implemented in a single COMSOL model. Figure 13 shows screen captures from the COMSOL interface showing an example of how such a model can be built. The *model builder* is shown in the middle of the figure. As explained in Sec. II C, three coupled physical interface are needed: two of them are *Magnetic field* interfaces, and the third one is a *Coefficient form PDE*. The magnetic fields interfaces mf2 and mf1 correspond to the real and effective systems, respectively. The Coefficient form PDE interface corresponds to the Landau-Lifshitz equation.

The correspondence between the symbols used in this paper and the symbols used in the example COMSOL model
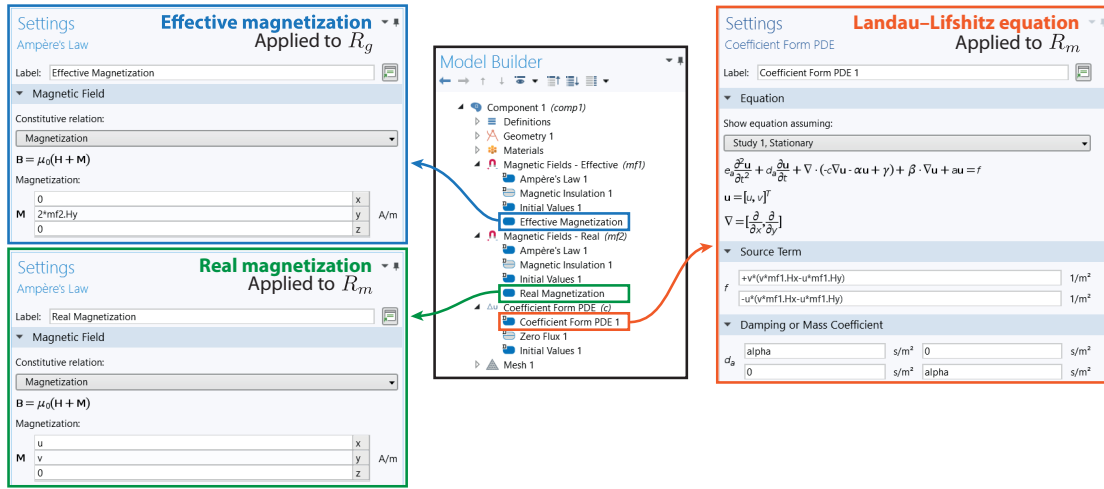
FIG. 13. Diagram of the structure of the COMSOL model, which corresponds to the implementation of the 2D example discussed in Sec. III A.

is given by

$$
\begin{aligned}
(\texttt{mf2.Hx}, \texttt{mf2.Hy}, \texttt{mf2.Hz})^T &\longleftrightarrow \mathbf{H} \\
(\texttt{mf2.Mx}, \texttt{mf2.My}, \texttt{mf2.Mz})^T &\longleftrightarrow \mathbf{M} \\
(\texttt{mf1.Hx}, \texttt{mf1.Hy}, \texttt{mf1.Hz})^T &\longleftrightarrow \mathbf{H}_{\text{eff}} \\
(\texttt{mf1.Mx}, \texttt{mf1.My}, \texttt{mf1.Mz})^T &\longleftrightarrow \mathbf{M}_{\text{eff}}
\end{aligned}
\tag{A1}
$$

Ampere's law node in $\texttt{mf1}$ corresponds to the effective magnetization. This is applied to the domains corresponding to the air-gap region R_g. Here, we input the analytical expression of the gradient of the objective $\mathcal{S}$ as a function of the real field. For the 2D example shown in Fig. 13, the problem is the same as the one presented in Sec. III A, i.e.,

$$
\mathbf{M}_{\text{eff}}(\mathbf{x}) = 2H_y(\mathbf{x})\hat{\mathbf{e}}_y. \tag{A2}
$$

This is shown in the top-left panel of Fig. 13. The objective functional $\mathcal{S}$ is only passed to COMSOL through the expression of the effective magnetization inserted here.

Ampere's law node in $\texttt{mf2}$ corresponds to the real magnetization, shown in the bottom-left panel of Fig. 13. This law is applied to the domains corresponding to the magnet region R_m. Since the evolution of the real magnetization is governed by the Landau-Lifshitz equation, the corresponding x and y components are, respectively, set to $\texttt{u}$ and $\texttt{v}$, i.e., the dependent variables of the Coefficient form PDE interface. For a three-dimensional example, the PDE interface would instead have three variables, corresponding to all the three vector components of $\mathbf{M}$.

The Coefficient form PDE interface is applied to the magnet region R_m. The differential equation governing $\texttt{u}$ and $\texttt{v}$ is shown in the right panel of Fig. 13. The only nonzero coefficients of the Coefficient form PDE are the

source term $\texttt{f}$ and the damping coefficient $\texttt{d}_a$. Therefore, written in the COMSOL notation, the equation reduces to

$$
\begin{aligned}
\texttt{d}_a \frac{\partial \texttt{u}}{\partial t} &= \texttt{f}_x \\
\texttt{d}_a \frac{\partial \texttt{v}}{\partial t} &= \texttt{f}_y
\end{aligned}
\tag{A3}
$$

where the damping coefficient $\texttt{d}_a$ is equal to $-1/\alpha$, and the source terms $\texttt{f}_x$ and $\texttt{f}_y$ are given by

$$
\begin{aligned}
\texttt{f}_x &= +\texttt{v} * (\texttt{v} * \texttt{mf1.Hx} - \texttt{u} * \texttt{mf1.Hy}) \\
\texttt{f}_y &= -\texttt{u} * (\texttt{v} * \texttt{mf1.Hx} - \texttt{u} * \texttt{mf1.Hy})
\end{aligned}
\tag{A4}
$$

Inspecting these expressions we can see that they correspond to the first two vector components of Eq. (15) for a two-dimensional case.

Finally, the COMSOL model includes a time-dependent study node that integrates the set of coupled partial differential equations. We use the direct MUMPS solver (multifrontal massively parallel sparse direct solver), with implicit time stepping using the BDF method (backward differentiation formula).

2. Examples of noncontinuous functionals

As a counterexample, let us consider the noncontinuous functional $\mathcal{Q}$:

$$
\mathcal{Q}[\mathbf{M}] = \max_{\mathbf{x}, \mathbf{x}' \in R_m} \|\mathbf{M}(\mathbf{x}) - \mathbf{M}(\mathbf{x}')\|. \tag{A5}
$$

In other words $\mathcal{Q}$ is the maximum norm of the difference between magnetization vectors at two different points. Let us apply the variation $\delta \mathbf{M}_1$ defined in Eq. (57) to a previously uniform magnetization distribution. Clearly, we

would get a finite variation $\delta\mathcal{Q} = \|\mathbf{\Delta}\|$ when changing $\mathbf{M}$ by a finite amount even if we do it in a single point. In fact, $\mathcal{Q}$ is not continuous with respect to $\mathbf{M}$ since $|\delta\mathcal{Q}|$ does not go to zero for $\|\delta\mathbf{M}_1\|_H \to 0$.

Let us now consider the functional $\mathcal{P}$ defined as

$$\mathcal{P}[\mathbf{M}] = \max_{\mathbf{x},\mathbf{x}' \in R_m : \mathbf{M}(\mathbf{x}) \neq \mathbf{M}(\mathbf{x}')} \|\mathbf{x} - \mathbf{x}'\|. \qquad (A6)$$

In other words $\mathcal{P}$ gives the maximum distance between points where the magnetization is not exactly the same. Let us apply the variation $\delta\mathbf{M}_2$ defined in Eq. (58) to a previously uniform magnetization distribution. Clearly, if $\mathbf{M}$ is changed over a finite region by an infinitesimal amount, the variation of $\mathcal{P}$ is finite. The variation $\delta\mathcal{P}$ is at maximum equal to the diameter of the set R_m. In conclusion, the functional $\mathcal{P}$ is also noncontinuous since $\|\delta\mathbf{M}_2\|_H \to 0$ for this variation.

3. Additional implementation details

In this Appendix we discuss in more detail the implementation of steps 1 and 3 of the iteration described in Sec. IV D. In order to do so, we introduce the scalar function $n : (R_m \subset \mathbb{R}^3) \to \mathbb{N}$ that gives the index of the region assigned to each point, i.e., $\mathbf{x} \in R_{n(\mathbf{x})}, \forall\mathbf{x}$. Therefore, the magnetization is defined as

$$\mathbf{M}(\mathbf{x}) = \mathbf{M}_n, \quad \forall\, \mathbf{x} \in R_n. \qquad (A7)$$

We define the N scalar functions $L_n(\mathbf{x})$ as

$$L_n(\mathbf{x}) = \mathbf{H}_{\mathrm{eff}}(\mathbf{x}) \cdot \mathbf{M}_n. \qquad (A8)$$

We also consider the n vectors $\langle\mathbf{H}_{\mathrm{eff}}\rangle_{R_n}$ that are the space averages of the effective field over the N regions:

$$\langle\mathbf{H}_{\mathrm{eff}}\rangle_{R_n} = \frac{1}{m(R_n)} \int_{R_n} dV \mathbf{H}_{\mathrm{eff}}(\mathbf{x}), \qquad (A9)$$

where $m(R_n)$ denotes the volume of the region R_n.

Here we will assume that the goal is to maximize $\mathcal{S}$. The same procedure applies to the case of minimization by replacing $\mathcal{S}$ with $-\mathcal{S}$. Below it is discussed how to update the N uniformly magnetized regions, and how to update the corresponding magnetization vectors.

Update regions: the regions are updated based on the value of the scalar function $\Delta(\mathbf{x})$ defined as

$$\Delta(\mathbf{x}) = \max_{n' \neq n(\mathbf{x})} \left(L_{n'}(\mathbf{x}) - L_{n(\mathbf{x})}(\mathbf{x}) \right). \qquad (A10)$$

As can be seen from Eqs. (54) and (A8), the function $\Delta(\mathbf{x})$ gives the potential improvement in reassigning a point $\mathbf{x} \in R_m$ to a different region. Our goal is to reassign a small subset of R_m to a different region than the current one. This set consists of those points that would give the maximum

improvement. We thus define the region $R(\delta)$ as the set of all points for which the potential improvement is greater than a certain value δ:

$$R(\delta) = \{\mathbf{x} \in R_m : \Delta(\mathbf{x}) \geq \delta\}. \qquad (A11)$$

It is convenient to consider the parameter $\alpha_{\mathrm{reg.}}$ corresponding to the volume of the reassigned region normalized by the volume of the maximum possible variation:

$$\frac{m(R(\delta))}{m(R(0))} = \alpha_{\mathrm{reg.}} \qquad (A12)$$

Note that $R(0)$ is the set of all the points that would benefit in being reassigned to a different segment other than the current one. In fact, when $\Delta(\mathbf{x})$ is negative there is no possible improvement in reassigning the point $\mathbf{x}$, since it is already in the best possible region. When we set $\alpha_{\mathrm{reg.}} = 0$ the regions are not evolving at all, vice versa when we set $\alpha_{\mathrm{reg.}} = 1$ the whole set $R(0)$ is reassigned, each point to the region giving the maximum improvement.

Update directions: the magnetization vectors of the N regions are updated based on the values of $\langle\mathbf{H}_{\mathrm{eff}}\rangle_{R_n}$. For each of the N regions, we introduce a rotation matrix $\underline{\underline{R}}_n(\theta)$. The rotation is performed around the axis $\mathbf{M}_n \times \langle\mathbf{H}_{\mathrm{eff}}\rangle_{R_n}$ by an angle θ_n. Each of the magnetization vectors is thus rotated according to

$$\mathbf{M}_n \to \underline{\underline{R}}_n(\theta_n)\mathbf{M}_n. \qquad (A13)$$

For each region, the maximum possible rotation that would give an improvement corresponds to the angle that would align $\mathbf{M}_n$ to $\langle\mathbf{H}_{\mathrm{eff}}\rangle_{R_n}$, i.e., the angle θ_n^* defined as

$$\theta_n^* = \mathrm{asin}\left(\frac{\|\mathbf{M}_n \times \langle\mathbf{H}_{\mathrm{eff}}\rangle_{R_n}\|}{\|\mathbf{M}_n\| \|\langle\mathbf{H}_{\mathrm{eff}}\rangle_{R_n}\|} \right). \qquad (A14)$$

It is convenient to introduce the parameter $\alpha_{\mathrm{dir.}}$ that determines the rotation of each of the N magnetization vectors normalized by the maximum rotation that would give an improvement:

$$\frac{\theta_n}{\theta_n^*} = \alpha_{\mathrm{dir.}} \qquad (A15)$$

When we set $\alpha_{\mathrm{dir.}} = 0$ the magnetization vectors $\mathbf{M}_n$ do not evolve at all, vice versa when we set $\alpha_{\mathrm{dir.}} = 1$ the rotation aligns each of the vectors to the average of the effective field over the corresponding region.

It is worth mentioning that in principle, the method for updating the regions described above allows topological changes to happen, for example, a region could become multiply connected. This is an undesirable outcome, since the solution does not correspond to the original problem. However, this did not occur for the considered examples. Our approach could be modified taking inspiration from the marching squares algorithm to avoid this problem entirely.

4. The adjoint method

a. Review of the method

We briefly review the idea behind the adjoint method. We consider a real-valued objective functional $\mathcal{S}_{\mathbf{v}} : \mathbb{U} \to \mathbb{R}$ defined over a Hilbert space $\mathbb{U}$. The subscript $\mathbf{v}$ indicates the explicit dependence of the functional on a design variable $\mathbf{v}$, which is an element of another Hilbert space $\mathbb{V}$. The argument of $\mathcal{S}_{\mathbf{v}}$ will be denoted by $\mathbf{u} \in \mathbb{U}$. This argument must satisfy a given constraint, also referred to as state equation, which is expressed as

$$\mathbf{F}_{\mathbf{v}}[\mathbf{u}] = \mathbf{L}_{\mathbf{v}}[\mathbf{u}] - \mathbf{w}_{\mathbf{v}} = \mathbf{0}. \qquad (A16)$$

Here $\mathbf{F}_{\mathbf{v}}$ and $\mathbf{L}_{\mathbf{v}}$ are operators $\mathbb{U} \to \mathbb{W}$, and we assume that $\mathbf{L}_{\mathbf{v}}$ is linear. The symbol $\mathbf{w}_{\mathbf{v}}$ denotes an element of the Hilbert space $\mathbb{W}$. Both $\mathbf{L}_{\mathbf{v}}$ and $\mathbf{w}_{\mathbf{v}}$ depend explicitly on the design variable $\mathbf{v}$.

Therefore, $\mathbf{u}$ depends implicitly on $\mathbf{v}$ via Eq. (A16). The purpose of the adjoint method is to calculate the total derivative of the optimization objective $\mathcal{S}$ with respect to the design variable $\mathbf{v}$. In order to do that, we introduce an additional variable $\boldsymbol{\lambda} \in \mathbb{W}$, defined implicitly via the following equation:

$$\nabla_{\mathbf{u}} \left(\mathcal{S}_{\mathbf{v}}[\mathbf{u}] + \boldsymbol{\lambda} \cdot \mathbf{F}_{\mathbf{v}}[\mathbf{u}] \right) = \mathbf{0}, \qquad (A17)$$

where the $\cdot$ operator denotes the inner product defined over the Hilbert space $\mathbb{W}$. From this point on, it will be convenient to imagine that all the elements of the Hilbert spaces $\mathbb{U}$, $\mathbb{V}$, and $\mathbb{W}$ are expanded over a corresponding basis. Therefore, we will express the equations in terms of the expansion coefficients of the vectors. This is equivalent to considering the weak formulation of the problem defined above. Analogously, the linear operator $\mathbf{L}$ will be expressed in matrix form. The dependence on $\mathbf{v}$ will be omitted when the subscript indexes are used. Equation (A17) is then expressed as

$$\frac{\partial \mathcal{S}_{\mathbf{v}}}{\partial u_i} + \frac{\partial}{\partial u_i} \left(\sum_j \lambda_j (\sum_{i'} L_{ji'} u_{i'} - \mathbf{w}_j) \right) = 0, \quad \forall i, \quad (A18)$$

$$\frac{\partial \mathcal{S}_{\mathbf{v}}}{\partial u_i} + \sum_j \lambda_j L_{ji} = \frac{\partial \mathcal{S}_{\mathbf{v}}}{\partial u_i} + \sum_j (L^T)_{ij} \lambda_j = 0, \qquad (A19)$$

$$\frac{\partial \mathcal{S}_{\mathbf{v}}}{\partial u_i} = -\sum_j (L^T)_{ij} \lambda_j. \qquad (A20)$$

Expressed in vector notation

$$\nabla_{\mathbf{u}} \mathcal{S}_{\mathbf{v}}[\mathbf{u}] = -\mathbf{L}_{\mathbf{v}}^T[\boldsymbol{\lambda}]. \qquad (A21)$$

This equation is analogous to Eq. (A16), with the substitutions $\mathbf{u} \to \boldsymbol{\lambda}$, $\mathbf{w} \to -\nabla_{\mathbf{u}} \mathcal{S}_{\mathbf{v}}[\mathbf{u}]$, and $\mathbf{L}_{\mathbf{v}} \to \mathbf{L}_{\mathbf{v}}^T$. In other words, $\boldsymbol{\lambda}$ satisfies the adjoint of the state equation, but with a different source term.

We now apply the total derivative with respect to $\mathbf{v}$ to Eq. (A16). This means that we are considering the implicit dependence of $\mathbf{u}$ on $\mathbf{v}$.

$$\frac{d}{dv_k} \left(\sum_i L_{ji} u_i - w_j \right) = 0, \quad \forall k, j, \qquad (A22)$$

$$\sum_i \left(\frac{\partial L_{ji}}{\partial v_k} u_i \right) - \left(\frac{\partial w_j}{\partial v_k} \right) = -\sum_i L_{ji} \frac{du_i}{dv_k}. \qquad (A23)$$

We are finally ready to calculate the derivative that we are interested in

$$\frac{d}{dv_k} \mathcal{S}_{\mathbf{v}}[\mathbf{u}] = \frac{\partial \mathcal{S}_{\mathbf{v}}}{\partial v_k}[\mathbf{u}] + \sum_i \frac{du_i}{dv_k} \frac{\partial \mathcal{S}_{\mathbf{v}}}{\partial u_i} \qquad (A24)$$

Using Eq. (A20) we obtain

$$\frac{d}{dv_k} \mathcal{S}_{\mathbf{v}}[\mathbf{u}] = \frac{\partial \mathcal{S}_{\mathbf{v}}}{\partial v_k}[\mathbf{u}] - \sum_i \frac{du_i}{dv_k} \left(\sum_j (L^T)_{ij} \lambda_j \right), \quad (A25)$$

$$\frac{d}{dv_k} \mathcal{S}_{\mathbf{v}}[\mathbf{u}] = \frac{\partial \mathcal{S}_{\mathbf{v}}}{\partial v_k}[\mathbf{u}] - \sum_j \lambda_j \left(\sum_i L_{ji} \frac{du_i}{dv_k} \right). \qquad (A26)$$

We now use Eq. (A23) to obtain the result

$$\frac{d}{dv_k} \mathcal{S}_{\mathbf{v}}[\mathbf{u}] = \frac{\partial \mathcal{S}_{\mathbf{v}}}{\partial v_k}[\mathbf{u}] + \sum_j \lambda_j \left(\sum_i \left(\frac{\partial L_{ji}}{\partial v_k} u_i \right) - \left(\frac{\partial w_j}{\partial v_k} \right) \right). \qquad (A27)$$

This equation is coupled to Eq. (A20) in the sense that $\boldsymbol{\lambda}$ is calculated by solving the adjoint equation before plugging it into Eq. (A27) to compute the desired derivative. This is the essence of the adjoint method.

b. Adjoint method and magnet design

When this method is applied to magnet design problems, the most widely used choice is to consider the field $\mathbf{u}$ to be the magnetic scalar potential V [8–10]. The state equation will then be Poisson's equation. Two main alternatives are then possible. The first option is that the magnetization is parametrized directly by the design variable $\mathbf{v}$, and the relation $\mathbf{B} = \mu_0(\mathbf{H} + \mathbf{M})$ is used. The second option is to use the constitutive relation $\mathbf{B} = \underline{\underline{\mu}}\mathbf{H} + \mathbf{B}_{\mathrm{rem}}$, in which case $\underline{\underline{\mu}}$ and the remanent flux density $\mathbf{B}_{\mathrm{rem}}$ may both depend on $\mathbf{v}$. These two alternatives lead to the corresponding state

equations:

$$\nabla^2 V = \nabla \cdot \mathbf{M}, \tag{A28}$$

or

$$\nabla \cdot \left(\underline{\underline{\mu}} \nabla V \right) = \nabla \cdot \mathbf{B}_{\text{rem}}. \tag{A29}$$

The latter choice has the advantage that the permeability tensor may also be dependent on the design variable $\mathbf{v}$, which is necessary when the shape of the iron parts need to be optimized. However, it should be stressed that this problem is intrinsically more difficult to solve due to the highly nonlinear dependence of $\mathbf{H}$ on $\underline{\underline{\mu}}(\mathbf{x})$.

In both cases, the fact that the operator $\mathbf{L}$ is self-adjoint is extremely convenient, which is equivalent to applying the reciprocity theorem. For the parametrization given by Eq. (A28), the $\mathbf{L}$ operator is the Laplace operator ∇^2, and $\mathbf{w_v}$ is the divergence of the magnetization. The adjoint equation is thus

$$\nabla^2 \lambda = \nabla_V S_{\mathbf{v}}[V] \tag{A30}$$

and Eq. (A27) becomes

$$\frac{d}{dv_k} S_{\mathbf{v}}[V] = \frac{\partial S_{\mathbf{v}}}{\partial v_k}[V] - \sum_j \lambda_j \left(\nabla \cdot \frac{\partial \mathbf{M}_j}{\partial v_k} \right), \tag{A31}$$

where the index j still refers to the coefficients of expansion of $\mathbf{M}(\mathbf{x})$ and $\lambda(\mathbf{x})$ over a basis. It is now convenient to select the continuous basis of all three-dimensional Dirac distributions $\delta^3(\mathbf{x})$, and replace the discrete index j with the continuous index $\mathbf{x}'$ and the summation over j with a volume integral.

In this work we assume that the design variable is the magnetization itself, which is a vector field over $\mathbb{R}^3$. Therefore, the index k is replaced by the continuous index $\mathbf{x}$ combined with the discrete index n, which runs over the three spatial dimensions. When expressed in terms of the continuous basis, the term $\nabla \cdot \partial \mathbf{M}_j / \partial v_k$ is thus replaced by $\sum_m \partial / \partial x'_n \delta_{nm} \delta^3(\mathbf{x} - \mathbf{x}')$. We also assume that the objective functional does not depend explicitly on $\mathbf{M}$, but only through V, implying that the first term on the right-hand side of Eq. (A31) vanishes. Therefore, Eq. (A31) is written as

$$\nabla_{M_n} S[V](\mathbf{x}) = -\int dV' \lambda(\mathbf{x}') \left(\sum_m \frac{\partial}{\partial x'_n} \delta_{nm} \delta^3(\mathbf{x} - \mathbf{x}') \right)$$
$$= -\int dV' \lambda(\mathbf{x}') \left(\frac{\partial}{\partial x'_n} \delta^3(\mathbf{x} - \mathbf{x}') \right). \tag{A32}$$

Applying a well-known property of the Dirac δ function, we can move the differentiation $\partial / \partial x'_n$ to the function $\lambda(\mathbf{x}')$,

thus obtaining

$$\nabla_{M_n} S[V](\mathbf{x}) = -\int dV' \delta^3(\mathbf{x} - \mathbf{x}') \frac{\partial}{\partial x'_n} \lambda(\mathbf{x}') = -\frac{\partial}{\partial x_n} \lambda(\mathbf{x}), \tag{A33}$$

where we used the definition of the Dirac δ function to solve the integral. When expressed in vector notation, the previous equation is written as

$$\nabla_{\mathbf{M}} S[V] = -\nabla \lambda. \tag{A34}$$

If we interpret λ as an effective magnetic scalar potential, V_{eff}, and the negative of its gradient as an effective field, then the last equation can be written as

$$\nabla_{\mathbf{M}} S[V] = \mathbf{H}_{\text{eff}}. \tag{A35}$$

The adjoint equation becomes

$$\nabla^2 V_{\text{eff}} = \nabla \cdot \mathbf{M}_{\text{eff}}, \tag{A36}$$

where we denoted by $\mathbf{M}_{\text{eff}}$ the derivative $\nabla_{\mathbf{H}} S$. This equation implies that the effective field is the field generated by the effective magnetization. In conclusion, the method presented in this paper can be seen as a particular case of the adjoint method, where the design variable is the magnetization vector field $\mathbf{M}$, itself.

---

[1] J. M. Coey, Permanent magnet applications, J. Magn. Magn. Mater. **248**, 441 (2002).

[2] A. Sarwar, A. Nemirovski, and B. Shapiro, Optimal Halbach permanent magnet designs for maximally pulling and pushing nanoparticles, J. Magn. Magn. Mater. **324**, 742 (2012).

[3] J. Lee, T. Nomura, and E. M. Dede, Topology optimization of magnetic composite microstructures for electropermanent magnet, J. Magn. Magn. Mater. **503**, 166596 (2020).

[4] J. Lee, J. Lee, T. Jung, and J. Yoo, Topology optimization for three-dimensional design of segmented permanent magnet arrays, Struct. Multidiscipl. Optim. **62**, 3089 (2020).

[5] R. Bjørk, C. Bahl, and A. Insinga, Topology optimized permanent magnet systems, J. Magn. Magn. Mater. **437**, 78 (2017).

[6] R. Bjørk and A. Insinga, A topology optimized switchable permanent magnet system, J. Magn. Magn. Mater. **465**, 106 (2018).

[7] R. Teyber, P. V. Trevizoli, T. V. Christiaanse, P. Govindappa, and A. Rowe, Topology optimization of reduced rare-earth permanent magnet arrays with finite coercivity, J. Appl. Phys. **123**, 193903 (2018).

[8] C. Abert, C. Huber, F. Bruckner, C. Vogler, G. Wautischer, and D. Suess, A fast finite-difference algorithm for topology optimization of permanent magnets, J. Appl. Phys. **122**, 113904 (2017).

[9] F. Bruckner, C. Abert, G. Wautischer, C. Huber, C. Vogler, M. Hinze, and D. Suess, Solving large-scale inverse magnetostatic problems using the adjoint method, Sci. Rep. **7**, 40816 (2017).

[10] G. Wautischer, C. Abert, F. Bruckner, F. Slanovc, and D. Suess, A topology optimization algorithm for magnetic structures based on a hybrid FEM-BEM method utilizing the adjoint approach, Sci. Rep. **12**, 1119 (2022).

[11] J. Lee, E. M. Dede, and T. Nomura, Simultaneous design optimization of permanent magnet, coils, and ferromagnetic material in actuators, IEEE Trans. Magn. **47**, 4712 (2011).

[12] J. Lee, E. M. Dede, D. Banerjee, and H. Iizuka, Magnetic force enhancement in a linear actuator by air-gap magnetic field distribution optimization and design, Finite Elem. Anal. Des. **58**, 44 (2012).

[13] A. A. Arkadan, Shape optimization of PM devices using constrained gradient based inverse problem methodology, IEEE Trans. Magn. **32**, 1222 (1996).

[14] A. Insinga, R. Bjørk, A. Smith, and C. Bahl, Globally optimal segmentation of permanent-magnet systems, Phys. Rev. Appl. **5**, 064014 (2016).

[15] A. Insinga, A. Smith, C. Bahl, K. Nielsen, and R. Bjørk, Optimal segmentation of three-dimensional permanent-magnet assemblies, Phys. Rev. Appl. **12**, 064034 (2019).

[16] J. D. Jackson, *Classical Electrodynamics* (Wiley, New York, NY, 1975), 2nd ed.

[17] P. F. Silva, M. Jouda, and J. G. Korvink, Magnetostatic reciprocity for MR magnet design, Magn. Reson. **2**, 607 (2021).

[18] S. C. Westmoreland, R. F. Evans, G. Hrkac, T. Schrefl, G. T. Zimanyi, M. Winklhofer, N. Sakuma, M. Yano, A. Kato, T. Shoji, A. Manabe, M. Ito, and R. W. Chantrell, Multiscale model approaches to the design of advanced permanent magnets, Scr. Mater. **148**, 56 (2018).

[19] S. Perna, F. Bruckner, C. Serpico, D. Suess, and M. d'Aquino, Computational micromagnetics based on normal modes: Bridging the gap between macrospin and full spatial discretization, J. Magn. Magn. Mater. **546**, 168683 (2022).

[20] M. d'Aquino, S. Perna, and C. Serpico, Micromagnetic study of statistical switching in magnetic tunnel junctions stabilized by perpendicular shape anisotropy, Phys. B: Condens. Matter **577**, 411744 (2020).

[21] J. Fischbacher, A. Kovacs, M. Gusenbauer, H. Oezelt, L. Exl, S. Bance, and T. Schrefl, Micromagnetics of rare-earth efficient permanent magnets, J. Phys. D: Appl. Phys. **51**, 193002 (2018).

[22] A. Insinga, E. Blaabjerg Poulsen, K. Nielsen, and R. Bjørk, A direct method to solve quasistatic micromagnetic problems, J. Magn. Magn. Mater. **510**, 166900 (2020).

[23] *Comsol multiphysics*, COMSOL AB, Stockholm, Sweden.

[24] R. Teyber, L. Brouwer, J. Qiang, and S. Prestemon, Inverse Biot-Savart optimization for superconducting accelerator magnets, IEEE Trans. Magn. **57**, 9465146 (2021).

[25] L. Debnath and P. Mikusinski, *Introduction to Hilbert Spaces with Applications* (Elsevier Science, Cambridge, Massachusetts, 2005).

[26] R. Bjørk, C. R. H. Bahl, A. Smith, D. Christensen, and N. Pryds, An optimized magnet for magnetic refrigeration, J. Magn. Magn. Mater. **322**, 3324 (2010).

[27] R. Bjørk, A. Smith, and C. R. H. Bahl, Analysis of the magnetic field, force, and torque for two-dimensional Halbach cylinders, J. Magn. Magn. Mater. **322**, 133 (2010).